

# UC Davis

## UC Davis Previously Published Works

### Title

Balance Between Rapid Delayed Rectifier K<sup>+</sup> Current and Late Na<sup>+</sup> Current on Ventricular Repolarization

### Permalink

<https://escholarship.org/uc/item/5jf2z029>

### Journal

Circulation Arrhythmia and Electrophysiology, 13(4)

### ISSN

1941-3149

### Authors

Hegyí, Bence

Chen-Izu, Ye

Izu, Leighton T

et al.

### Publication Date

2020-04-01

### DOI

10.1161/circep.119.008130

Peer reviewed



Published in final edited form as:

*Circ Arrhythm Electrophysiol.* 2020 April ; 13(4): e008130. doi:10.1161/CIRCEP.119.008130.

## Balance Between Rapid Delayed Rectifier K<sup>+</sup> Current and Late Na<sup>+</sup> Current on Ventricular Repolarization: An Effective Antiarrhythmic Target?

Bence Hegyi, MD, PhD<sup>1</sup>, Ye Chen-Izu, PhD<sup>1,2,3</sup>, Leighton T. Izu, PhD<sup>1</sup>, Sridharan Rajamani, PhD<sup>4</sup>, Luiz Belardinelli, MD<sup>5</sup>, Donald M. Bers, PhD<sup>1</sup>, Tamás Bányász, MD, PhD<sup>1,6</sup>

<sup>1</sup>Department of Pharmacology, University of California, Davis

<sup>2</sup>Department of Biomedical Engineering, University of California, Davis

<sup>3</sup>Department of Internal Medicine/Cardiology, University of California, Davis

<sup>4</sup>Amgen, Inc., South San Francisco, University of Debrecen, Debrecen, Hungary

<sup>5</sup>InCarda Therapeutics, Inc., Newark, CA, University of Debrecen, Debrecen, Hungary

<sup>6</sup>Department of Physiology, Faculty of Medicine, University of Debrecen, Debrecen, Hungary

### Abstract

**Background**—Rapid delayed rectifier K<sup>+</sup> current ( $I_{Kr}$ ) and late Na<sup>+</sup> current ( $I_{NaL}$ ) significantly shape the cardiac action potential (AP). Changes in their magnitudes can cause either long or short QT syndromes (LQT, SQT) associated with malignant ventricular arrhythmias and sudden cardiac death.

**Methods**—Physiological self AP-clamp was used to measure  $I_{NaL}$  and  $I_{Kr}$  during the AP in rabbit and porcine ventricular cardiomyocytes in order to test our hypothesis that the balance between  $I_{Kr}$  and  $I_{NaL}$  affects repolarization stability in health and disease conditions.

**Results**—We found comparable amount of net charge carried by  $I_{Kr}$  and  $I_{NaL}$  during the physiological AP suggesting that outward K<sup>+</sup> current via  $I_{Kr}$  and inward Na<sup>+</sup> current via  $I_{NaL}$  are in balance during physiological repolarization. Remarkably,  $I_{Kr}$  and  $I_{NaL}$  integrals in each control myocyte were highly correlated in both healthy rabbit and pig myocytes, despite high overall cell-to-cell variability. This close correlation was lost in heart failure myocytes from both species. Pretreatment with E-4031 to block  $I_{Kr}$  (mimicking LQT2) or with ATX-II to impair Na<sup>+</sup> channel inactivation (mimicking LQT3) prolonged APD; however, using GS-967 to inhibit  $I_{NaL}$  sufficiently restored APD to control in both cases. Importantly,  $I_{NaL}$  inhibition significantly reduced the beat-to-beat and short-term variabilities of APD. Moreover,  $I_{NaL}$  inhibition also restored APD and repolarization stability in heart failure. Conversely, pretreatment with GS-967 shortened APD (mimicking SQT), and E-4031 reverted APD shortening. Furthermore, the

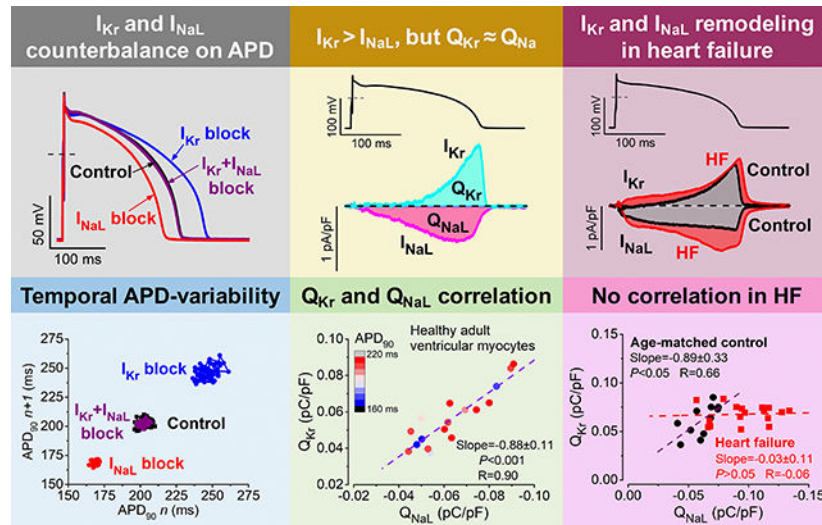
**Correspondence:** Bence Hegyi, MD, PhD, Department of Pharmacology, University of California, Davis, 451 Health Sciences Drive, Davis, CA 95616, Tel: +1-530-752-9962, Fax: +1-530-752-7710, bhegyi@ucdavis.edu.

**Disclosures:** Dr. Luiz Belardinelli and Dr. Sridharan Rajamani are former employees of Gilead Sciences, Inc. (Foster City, CA, USA), which is the patent holder of GS-967. The other authors report no conflicts.

amplitude of AP alternans occurring at high pacing frequency was decreased by  $I_{NaL}$  inhibition, increased by  $I_{Kr}$  inhibition, and restored by combined  $I_{NaL}$  and  $I_{Kr}$  inhibitions.

**Conclusions**—Our data demonstrate that  $I_{Kr}$  and  $I_{NaL}$  are counterbalancing currents during the physiological ventricular AP and their integrals co-vary in individual myocytes. Targeting these ionic currents to normalize their balance may have significant therapeutic potential in heart diseases with repolarization abnormalities.

## Graphical Abstract



## Keywords

action potential; HERG arrhythmia; Na<sup>+</sup> current; heart; repolarization; repolarization stability; late sodium current; rapid delayed rectifier potassium current

## Introduction

The shape of the cardiac action potential (AP) is determined by an integrative process between various depolarizing and repolarizing ionic currents. Pathological alterations in their balance may result in either prolongation or shortening of AP duration (APD) manifested as long or short QT interval in the electrocardiogram.<sup>1</sup> The rapid delayed rectifier K<sup>+</sup> current ( $I_{Kr}$ ) and the late Na<sup>+</sup> current ( $I_{NaL}$ ) significantly affect AP repolarization, thus contributing to regulation of the APD.<sup>2</sup> Accordingly, both reduced  $I_{Kr}$  and increased  $I_{NaL}$  are known to cause long QT syndrome (LQT2 and LQT3, respectively), a clinical condition associated with increased risk for torsades de pointes-type ventricular tachycardia.<sup>2</sup> On the contrary, gain-of-function mutations in hERG (K<sub>v</sub>11.1 channel, increased  $I_{Kr}$ ) and loss-of-function mutations in SCN5A (Na<sub>v</sub>1.5 channels, decreased  $I_{NaL}$ ) can lead to short QT syndrome (SQT) and Brugada syndrome (BrS).<sup>3,4</sup>

Cellular electrophysiological<sup>5,6</sup> and modeling studies<sup>7,8</sup> demonstrate that both  $I_{Kr}$  and  $I_{NaL}$  are activated during phase 3 of the ventricular AP and it has been proposed that  $I_{Kr}$  and  $I_{NaL}$  may counterbalance each other during physiological repolarization.<sup>7,9–11</sup> Although this

concept has not been systematically tested yet and supporting experimental data are sparse. Moreover, APD and plateau height are critical determinants of  $I_{K_r}$  and  $I_{NaL}$  densities and net charges under the AP.<sup>5</sup> Consequently, APD prolongation may facilitate  $I_{K_r}$  and  $I_{NaL}$  accumulation during the AP, whereas  $I_{K_r}$  and  $I_{NaL}$  can be reduced when APD is shortened. Therefore, we aimed to compare the impact of  $I_{K_r}$  and  $I_{NaL}$  on ventricular repolarization in health and disease. Clinical findings also support such concept, because treatments with mexiletine,<sup>12,13</sup> ranolazine<sup>14</sup> and hydroquinidine,<sup>15,16</sup> which may restore the balance between  $I_{K_r}$  and  $I_{NaL}$  can be beneficial in selected LQT, SQT and BrS patients. We hypothesized that the  $I_{K_r}/I_{NaL}$  balance, as previously proposed,<sup>7,9–11</sup> is a critical determinant of APD and targeting this balance may represent a novel antiarrhythmic strategy.

We systematically measured APs and ionic currents in rabbit and porcine ventricular cardiomyocytes using physiological self AP-clamp technique<sup>17</sup> in control, in pharmacologically-induced APD prolongation and shortening (modeling LQT and SQT), and in congestive heart failure (HF) induced by combined pressure/volume overload in rabbits<sup>18</sup> and by chronic myocardial infarction (MI) in pigs.<sup>6</sup> We also tested the relative contributions of  $I_{K_r}$  and  $I_{NaL}$  to the stability of APD in health and disease, because the increased beat-to-beat and short-term variabilities of APD can be better predictors of cardiac arrhythmias than the steady-state APD alone.<sup>19</sup> The mechanistic understanding of the relationship between  $I_{K_r}$  and  $I_{NaL}$  to set repolarization stability in cardiac health and disease may lead to more rational drug therapies.

## Methods

The data that support the findings of this study are available from the corresponding author upon reasonable request.

All animal handling and laboratory procedures were in accordance with the approved protocols (#20867 and #21137) of the local Institutional Animal Care and Use Committee conforming to the Guide for the Care and Use of Laboratory Animals published by the US National Institute of Health (8th edition, 2011). Chemicals and reagents were purchased from Sigma-Aldrich Co. (St. Louis, MO, USA) if not specified otherwise. GS-967 was obtained from Gilead Sciences, Inc. (Foster City, CA, USA) and E-4031 was from Tocris Bioscience (Bristol, UK).

### Animal models and cell isolation

Ventricular cardiomyocytes were isolated from 20 New Zealand White rabbits (male, 4-month-old) using a standard enzymatic technique with collagenase type II (Worthington Biochemical Co., Lakewood, NJ, USA) and protease type XIV (Sigma-Aldrich) as previously described.<sup>20</sup>

HF was induced in New Zealand White rabbits (male, 4-month-old) by aortic insufficiency and 4 weeks later by aortic constriction as previously described.<sup>18,21,22</sup> Data here reported was obtained from 6 HF and 4 age-matched control (AM) rabbits. HF progression was monitored periodically by echocardiography. Cardiomyocytes were isolated from rabbits at 2–2.5 years of age when left ventricular end-systolic dimension exceeded 1.45 cm (detailed

morphometric and echocardiography data are shown in Table I in the Data Supplement).<sup>18</sup> Cardiomyocytes isolated from healthy AM rabbits were used in control experiments.

Yucatan mini-pigs (male, 4- to 6-month-old) were subjected to microbead embolization of the first diagonal branch of the left anterior descending coronary artery, which caused transmural MI and progressive reduction in ejection fraction over 5 months (from the pre-operative  $68.1 \pm 3.9\%$  to  $44.2 \pm 4.9\%$ ,  $N=6$  animals,  $P < 0.01$ ), providing a clinically relevant large animal ischemic cardiomyopathy model as previously described.<sup>6</sup> Cardiomyocytes were isolated from the remote zone of the infarct ( $>2$  cm from the infarcted region) 5 months post-MI. As control, cardiomyocytes were isolated from the same region of the heart of 4 healthy, age-matched sham control mini-pigs.

### Electrophysiology

Recordings were performed in isolated ventricular cardiomyocytes using whole-cell patch-clamp with physiological solutions at  $36 \pm 0.1^\circ\text{C}$  (for ionic composition, see Data Supplement). APs were evoked in current-clamp experiments where cells were stimulated with short suprathreshold depolarizing pulses at 1 to 5 Hz pacing frequencies delivered via the patch pipette. Fifty consecutive APs were recorded to examine the average behavior at each pacing frequency. Short-term variability (STV) of AP duration measured at 90% of repolarization ( $\text{APD}_{90}$ ) was calculated according to the following formula:  $\text{STV} = \Sigma(|\text{APD}_{i+1} - \text{APD}_i|) / [(n_{\text{beats}} - 1) \times 2]$ , where  $\text{APD}_i$  and  $\text{APD}_{i+1}$  indicate the  $i^{\text{th}}$  and  $(i+1)^{\text{th}}$   $\text{APD}_{90}$  values, respectively, and  $n_{\text{beats}}$  denotes the number of consecutive beats analyzed.<sup>23</sup> Changes in STV are presented as Poincaré plots, where 50 consecutive  $\text{APD}_{90}$  values are plotted, each against the previous  $\text{APD}_{90}$ . To analyze further the variability of repolarization, the difference between consecutive  $\text{APD}_{90}$  values were grouped in milliseconds ranges and the overall probability of their appearance was calculated in each cell. Then these data were plotted in cumulative distribution curves to illustrate the changes in beat-to-beat variability of  $\text{APD}_{90}$ .<sup>24</sup>

Ionic currents during the AP were measured using self AP-clamp (at 2 Hz pacing in rabbits, and at 1 Hz in pigs) with physiological solutions, preserved  $[\text{Ca}^{2+}]_i$  cycling, and sequential block of specific ionic currents using selective ion channel inhibitors (Table II in the Data Supplement), as previously described.<sup>6,17</sup> A representative example is shown in Figure 1. E-4031 (1  $\mu\text{mol/L}$ ) and GS-967 (1  $\mu\text{mol/L}$ ) have been used to inhibit  $\text{I}_{\text{Kr}}$  and  $\text{I}_{\text{NaL}}$ , respectively.

### Statistical analysis

Data are expressed as Mean  $\pm$  SEM. The number of cells in each experimental group was reported as  $n/N = \text{number of cells/number of animals}$ . Statistical significance of differences was evaluated using paired Student  $t$  test or ANOVA with Bonferroni posttest as appropriate. Differences were deemed significant if  $P < 0.05$ .

## Results

### Profile of the major ionic currents under physiological AP-clamp

In order to assess the potential impact of  $I_{K_r}$  and  $I_{NaL}$  on AP repolarization, first we recorded the major depolarizing and repolarizing ionic currents in rabbit ventricular cardiomyocytes under physiological self AP-clamp and sequential dissection of ionic currents using selective ion channel inhibitors (Table II in the Data Supplement). Each ionic current has its characteristic profile and magnitude during the AP shown in Figure 1. The rapid opening of voltage-gated  $Na^+$  channels generates a transient  $Na^+$  current ( $I_{NaT}$ ) which is responsible for AP upstroke. The phase 1 repolarization of the AP is mediated by both the transient outward  $K^+$  current ( $I_{to}$ ) and the  $Ca^{2+}$ -activated  $Cl^-$  current ( $I_{Cl(Ca)}$ ). During AP plateau phase, a small sustained  $I_{NaL}$  and a significantly larger but more rapidly inactivating L-type  $Ca^{2+}$  current ( $I_{CaL}$ ) are the predominant inward currents (Figure 1). Phase 3 repolarization is predominantly mediated by  $I_{K_r}$ , and then the inward rectifier  $K^+$  current ( $I_{K1}$ ) completes terminal repolarization (Figure 1). The slow delayed rectifier  $K^+$  current ( $I_{Ks}$ ) and the  $Ca^{2+}$ -activated slow conductance (SK)  $K^+$  current ( $I_{K(Ca)}$ ) are small currents under a physiological ventricular AP in the absence of  $\beta$ -adrenergic stimulation. A significantly inward  $Na^+/Ca^{2+}$  exchanger (NCX) current ( $Ca^{2+}$  removal) is present during (and even after) terminal repolarization. Importantly, relatively small ionic currents are flowing and balancing each other during the plateau phase of the AP. Two key ionic currents,  $I_{K_r}$  and  $I_{NaL}$  achieve their peak density during the end of the plateau phase (Figure 1) suggesting that these currents may significantly influence APD and repolarization stability. Therefore, we focused on the mechanistic investigation of the relationship between  $I_{K_r}$  and  $I_{NaL}$  during normal and impaired repolarization.

### Profile of $I_{K_r}$ and $I_{NaL}$ during control, shortened and prolonged APD

We recorded  $I_{K_r}$  and  $I_{NaL}$  during the cell's own AP shown in Figure 2 using self AP-clamp with physiological solutions, at  $36^\circ C$  and 2 Hz steady-state pacing frequency. In control,  $I_{K_r}$  is rapidly activated during the phase 3 repolarization of the AP achieving a peak density of  $0.84 \pm 0.05$  pA/pF (Figure 2A). In contrast, a persistent  $I_{NaL}$  was present throughout the entire AP plateau; however,  $I_{NaL}$  achieved a peak density of  $-0.55 \pm 0.03$  pA/pF (35% less than  $I_{K_r}$  magnitude,  $P < 0.001$ ) also at the phase 3 of the AP when the driving force for  $Na^+$  entry is increased. Although  $I_{NaL}$  rises earlier than  $I_{K_r}$  during the AP plateau (Figure 2A), the net charge carried by  $I_{NaL}$  versus  $I_{K_r}$  during the AP were similar (Figure 2E and 2F inset;  $0.056 \pm 0.004$  versus  $0.063 \pm 0.004$  pC/pF, respectively;  $P = 0.17$ ). Even more striking is that the integrated  $I_{NaL}$  and  $I_{K_r}$  fluxes co-vary in individual cells, independent of APD (Figure 2I and 2J) which raises the possibility that channel expression might co-vary (see below).

In another set of experiments, cell pretreatment with  $I_{K_r}$  inhibitor E-4031 (1  $\mu$ mol/L) prolonged APD (pharmacologically induced LQT2 model). Self AP-clamp using prolonged APD (Figure 2B) led to increased  $I_{NaL}$  peak density (by 26%) and net charge (by 88%) versus control (Figure 2E and 2F). Next, pretreatment of the cell with the  $I_{NaL}$  inhibitor GS-967 (1  $\mu$ mol/L) shortened APD (pharmacologically induced SQT model). Self AP-clamp using shortened APD (Figure 2C) led to reduced  $I_{K_r}$  peak density (by 23%) and net charge (by 47%) versus control (Figure 2E and 2F). Sea anemone toxin II (ATX-II, 5 nmol/L) that

impairs Na<sup>+</sup> channel inactivation prolonged APD (pharmacologically induced LQT3 model) and markedly increased I<sub>NaL</sub> under self AP-clamp (Figure 2D). ATX-II increased I<sub>NaL</sub> peak density by 148% and net charge by 268% versus control; however, the prolonged APD by ATX-II also led to increased I<sub>Kr</sub> peak density by 32% and net charge by 113% versus control (Figure 2E and 2F). These acute manipulations of I<sub>Kr</sub> and I<sub>NaL</sub> and APD exemplify that in addition to the co-varying I<sub>Kr</sub> and I<sub>NaL</sub> at baseline, the acute changes in APD evoke inherent biophysical coordination between I<sub>Kr</sub> and I<sub>NaL</sub> (Figure 2G and 2H). That is, if APD is prolonged by excess I<sub>NaL</sub>, the long APD promotes more I<sub>Kr</sub> to limit APD prolongation.

Further analyzing the relationship between I<sub>Kr</sub> and I<sub>NaL</sub>, there was a more than 2-fold variation in both I<sub>Kr</sub> and I<sub>NaL</sub> magnitudes under self AP-clamp already in control cells (Figure 2I and 2J). Peak current densities in control varied in individual myocytes between 0.62 to 1.29 pA/pF and 0.35 to 0.84 pA/pF for I<sub>Kr</sub> and I<sub>NaL</sub>, respectively (Figure 2I). However, there was no correlation in control between the cells' baseline APD measured at 90% of repolarization (APD<sub>90</sub>) and either I<sub>Kr</sub> and I<sub>NaL</sub> peak densities (Figure 2I) or total charges (Figure 2J) under self AP-clamp. Despite the large cell-to-cell variability, I<sub>Kr</sub> and I<sub>NaL</sub> magnitudes were not randomly distributed, but instead I<sub>Kr</sub> and I<sub>NaL</sub> peak densities and net charges were highly correlated when measured in the same cell under self AP-clamp (Figure 2K and 2L). It also showed that similar APD<sub>90</sub> (or APD<sub>25</sub> or APD<sub>50</sub>, Figure I in the Data Supplement) can be generated by largely different, but matched I<sub>Kr</sub> and I<sub>NaL</sub> densities and net charges. These data suggest that I<sub>Kr</sub> and I<sub>NaL</sub> might be co-regulated not only biophysically but also in their functional expression.

### Altered I<sub>NaL</sub>/I<sub>Kr</sub> balance in HF

HF is known to be associated with arrhythmogenic electrophysiological remodeling including changes in I<sub>NaL</sub> and I<sub>Kr</sub> that leads to APD prolongation.<sup>18, 22</sup> We measured the profiles of I<sub>Kr</sub> and I<sub>NaL</sub> in HF versus AM under the same, precordated, typical rabbit AP (canonical AP-clamp; Figure 3). I<sub>NaL</sub> peak density was markedly increased in HF versus AM ( $-0.94 \pm 0.03$  versus  $-0.51 \pm 0.01$  pA/pF,  $P < 0.001$ ), whereas I<sub>Kr</sub> peak density was slightly increased in HF versus AM ( $1.13 \pm 0.02$  versus  $0.96 \pm 0.02$  pA/pF,  $P < 0.001$ ) under canonical AP-clamp shown in Figure 3A through 3D. This resulted in a 58% increase of I<sub>NaL</sub> net charge in contrast to 29% increase of I<sub>Kr</sub> net charge in HF versus AM (Figure 3C and 3D). Therefore, the balance between I<sub>NaL</sub> and I<sub>Kr</sub> is shifted toward enhanced depolarization in HF. Further analysis revealed that a significant correlation between I<sub>Kr</sub> and I<sub>NaL</sub> magnitudes in AM (ie, larger I<sub>Kr</sub> in those cells having larger I<sub>NaL</sub>) occurs not only in self AP-clamp (Figure 2K and 2L) but also under a canonical AP-clamp (Figure 3E and 3F). Importantly, this correlation was lost in HF and rather an opposite tendency was found (ie, reduced I<sub>Kr</sub> is concurrent with larger I<sub>NaL</sub>) under AP-clamp (Figure 3E and 3F), which may reflect the altered regulation and remodeling of the channels in HF. HF is characterized by impaired intracellular Ca<sup>2+</sup> handling and Ca<sup>2+</sup>-dependent signaling including upregulation of Ca<sup>2+</sup>/calmodulin-dependent protein kinase II (CaMKII).<sup>25</sup> Therefore, we repeated I<sub>NaL</sub> and I<sub>Kr</sub> measurements using 10 mmol/L BAPTA in the pipette in order to buffer [Ca<sup>2+</sup>]<sub>i</sub> to nominally zero (Figure II in the Data Supplement). BAPTA significantly reduced I<sub>NaL</sub> peak density in HF ( $-0.72 \pm 0.03$  pA/pF,  $P < 0.001$ ) but not in AM (Figure 3C). Moreover, BAPTA

slightly reduced  $I_{K_r}$  in HF versus AM ( $0.88 \pm 0.01$  pA/pF,  $P < 0.001$ ), whereas  $I_{K_r}$  was not changed by BAPTA in AM (Figure 3D).

### $I_{K_r}$ and $I_{NaL}$ counterbalance under control, shortened and prolonged APD

We tested the impact of  $I_{K_r}$  and  $I_{NaL}$  inhibition on APD in control and disease models. The  $I_{K_r}$  inhibitor E-4031 (1  $\mu$ mol/L) significantly prolonged APD<sub>90</sub> in healthy rabbit ventricular cardiomyocytes ( $245.1 \pm 5.8$  versus  $201.0 \pm 5.1$  ms,  $P < 0.001$ ) shown in Figure 4A. E-4031 affected the phase 3 repolarization (Figure 4E) of the AP by increasing the plateau potential measured at 75% of APD<sub>90</sub> (Plateau<sub>75</sub>) and decreasing the maximal rate of repolarization ( $-dV/dt_{max}$ ). Application of the  $I_{NaL}$  inhibitor GS-967 (1  $\mu$ mol/L) in the E-4031 pretreated cells shortened APD<sub>90</sub> back to control ( $199.7 \pm 6.6$  ms,  $P = 0.58$ ) by increasing  $-dV/dt_{max}$  (Figure 4A and 4E). Next, reversing the order of the treatments,  $I_{NaL}$  inhibition using GS-967 significantly shortened APD<sub>90</sub> in control ( $177.3 \pm 5.1$  versus  $206.9 \pm 2.6$  ms,  $P < 0.001$ ) shown in Figure 4B. GS-967 slightly depressed AP plateau potentials and accelerated phase 3 (Figure 4B and 4F). However, inhibiting  $I_{K_r}$  following GS-967 treatment restored APD<sub>90</sub> again to control ( $209.0 \pm 4.0$  ms,  $P = 0.66$  versus control).

In another cellular model of long QT, ATX-II (5 nmol/L) treatment was used to enhance  $I_{NaL}$  and significantly prolong APD<sub>90</sub> ( $265.1 \pm 8.9$  vs.  $201.5 \pm 3.2$  ms,  $P < 0.001$ ) shown in Figure 4C. ATX-II increased Plateau<sub>75</sub> as expected, but interestingly, ATX-II also accelerated the rate of repolarization (Figure 4G) in line with  $I_{K_r}$  accumulation under the elevated AP plateau and prolonged APD.  $I_{NaL}$  inhibitor GS-967 at a concentration of 100 nmol/L significantly shortened APD<sub>90</sub> following ATX-II treatment ( $222.4 \pm 6.7$  ms,  $P < 0.01$  versus ATX-II only), whereas a higher concentration of GS-967 (1  $\mu$ mol/L) abolished the ATX-II induced APD<sub>90</sub> prolongation ( $189.6 \pm 5.8$  ms,  $P = 0.07$  versus control) and reduced Plateau<sub>75</sub> to control (Figure 4G).  $I_{NaL}$  was also enhanced in HF (Figure 3) and APD<sub>90</sub> was prolonged in HF versus AM ( $253.1 \pm 18.5$  versus  $202.4 \pm 5.8$  ms,  $P < 0.05$ ) shown in Figure 4D. Importantly, the  $I_{NaL}$  inhibitor GS-967 (1  $\mu$ mol/L) shortened APD<sub>90</sub> in HF back to control ( $215.9 \pm 16.6$  ms,  $P > 0.05$  versus control) and increased  $-dV/dt_{max}$  (Figure 4H).

### Impact of $I_{K_r}$ and $I_{NaL}$ on repolarization stability

Next, we tested the contribution of  $I_{K_r}$  and  $I_{NaL}$  to the temporal dispersion of APD to assess repolarization stability.  $I_{K_r}$  inhibition (E-4031, 1  $\mu$ mol/L) significantly increased the short-term variability (STV) of APD<sub>90</sub> ( $3.6 \pm 0.4$  versus  $2.5 \pm 0.1$  ms,  $P < 0.001$ ), whereas  $I_{NaL}$  inhibition (GS-967, 1  $\mu$ mol/L) significantly decreased STV ( $1.6 \pm 0.1$  versus  $2.6 \pm 0.2$  ms,  $P < 0.001$ ) shown in Figure 5A and 5B in line with their effect on averaged APD<sub>90</sub> (Figure 4). However, combined  $I_{K_r} + I_{NaL}$  inhibition reduced STV below control ( $1.9 \pm 0.2$  ms,  $P < 0.001$ ), despite the unchanged averaged APD<sub>90</sub>. ATX-II robustly increased STV ( $5.0 \pm 0.6$  versus  $2.2 \pm 0.1$  ms,  $P < 0.001$ ) shown in Figure 5C. Interestingly, partial blockade (0.1  $\mu$ mol/L GS-967) of the enhanced  $I_{NaL}$  (by ATX-II) reduced STV to control ( $2.6 \pm 0.3$  ms,  $P > 0.05$  versus control), while APD<sub>90</sub> was still significantly prolonged (compare Figures 5C and 4C). Moreover, higher concentration of GS-967 (1  $\mu$ mol/L) decreased STV below control ( $1.7 \pm 0.2$  ms,  $P < 0.05$  versus control) even in the presence of ATX-II (Figure 5C). STV was also markedly increased in HF versus AM ( $4.4 \pm 0.5$  versus  $2.6 \pm 0.3$  ms,  $P < 0.05$ ) and

importantly  $I_{NaL}$  inhibition restored not only  $APD_{90}$  but also STV to control ( $2.7 \pm 0.4$  ms,  $P > 0.05$  versus AM) shown in Figure 5D.

To further analyze the beat-to-beat variability of  $APD_{90}$ , cumulative distribution of  $APD_{90}$ -variability in consecutive beats was calculated (Figure 5E through 5H). It showed that  $I_{Kr}$  inhibition (E-4031, 1  $\mu\text{mol/L}$ ) enhanced STV by markedly increasing the number of beats having large differences between consecutive  $APD_{90}$  values ( $>5$  and  $>10$  ms) (shown as long tails in the distribution curve), but the median beat-to-beat variability was similar to control (Figure 5E). However,  $I_{NaL}$  inhibition decreased both the median beat-to-beat variability and markedly reduced the number of APs having large differences in  $APD_{90}$  values in consecutive beats (Figure 5F). In agreement with this role of  $I_{NaL}$ , ATX-II treatment significantly increased both the median and large  $APD_{90}$  beat-to-beat variabilities in consecutive beats, which were then reverted by GS-967 (Figure 5G). Similarly, significantly enhanced beat-to-beat  $APD_{90}$ -variability was found in HF just as in ATX-II, and  $I_{NaL}$  inhibition significantly reduced beat-to-beat repolarization variability in HF (Figure 5H).

### Frequency-dependence of $I_{Kr}$ and $I_{NaL}$ inhibition

We also examined the frequency-dependence of  $I_{Kr}$  and  $I_{NaL}$  inhibition.  $I_{Kr}$  inhibition (E-4031, 1  $\mu\text{mol/L}$ ) caused a reverse-rate dependent lengthening of the  $APD_{90}$  (Figure 6A), and further analysis revealed that the observed  $APD_{90}$  prolongation was rather dependent on baseline  $APD_{90}$  (Figure 6C). Surprisingly,  $I_{NaL}$  inhibition (GS-967, 1  $\mu\text{mol/L}$ ) induced more pronounced APD shortening at higher pacing rates (Figure 6B). This positive rate-dependence of GS-967 effect on  $APD_{90}$  (Figure 6D) is the opposite to that expected based on the reduced  $\text{Na}^+$  channel availability, but the use-dependent drug-binding and the significant CaMKII-dependent modulation of  $I_{NaL}$  may be more important at rapid pacing rates.

In rabbit ventricular myocytes APD alternans occurred at high pacing rates (at 5 Hz at  $36^\circ\text{C}$ ). The amplitude of the APD alternans was increased by  $I_{Kr}$  inhibition and decreased by  $I_{NaL}$  inhibition (Figure 6E and 6F). Interestingly, during APD alternans only the long  $APD_{90}$  but not the short  $APD_{90}$  was altered by either E-4031 or GS-967. Moreover, GS-967 treatment transiently abolished APD alternans, then the magnitude of the APD alternans (the difference between long and short APDs) achieved a steady-state (in 60–90 seconds) at a reduced level compared to control (Figure 6F). This observation may reflect changes in  $[\text{Na}^+]_i$  and  $[\text{Ca}^{2+}]_i$ , which require further investigation. Importantly, combined application of E-4031 and GS-967 restored the magnitude of APD alternans at 5 Hz to control (Figure 6G and 6H), suggesting a counterbalance between  $I_{Kr}$  and  $I_{NaL}$  also at high pacing rates.

### Relationship between $I_{Kr}$ and $I_{NaL}$ in control and ischemic HF pigs

Next, we tested whether the correlation between  $I_{Kr}$  and  $I_{NaL}$  is present in another large animal model relevant to human electrophysiology.  $I_{NaL}$  measured under physiological self AP-clamp in control porcine ventricular myocytes was smaller ( $-0.33 \pm 0.01$  pA/pF), whereas  $I_{Kr}$  density was slightly larger ( $0.99 \pm 0.04$  pA/pF) than those measured in rabbit (compare Figure 7 and Figure 2). However,  $I_{NaL}$  total charge ( $0.050 \pm 0.004$  pC/pF) was still similar to that measured in rabbits because of the longer  $APD_{90}$  ( $227.9 \pm 17.7$  ms) in pigs (Figure 7C).

Importantly, we found statistically significant correlation between both peak densities and total charges of  $I_{NaL}$  and  $I_{Kr}$  under self AP-clamp also in pigs (Figure 7E and 7F).

Chronic ischemic HF (5 months post-MI) in pigs led to APD<sub>90</sub> prolongation ( $246.1 \pm 12.9$  ms) and remodeling in both  $I_{NaL}$  and  $I_{Kr}$  in myocytes isolated from the remote zone of the infarct (Figure 7B). However,  $I_{NaL}$  was only slightly increased (by 38%) in porcine ischemic HF (Figure 7C), whereas  $I_{NaL}$  was markedly increased (by 84%) in nonischemic (volume/pressure-overload) rabbit HF (Figure 3C). In the same time,  $I_{Kr}$  decreased by 13% in porcine ischemic HF (Figure 7D) as opposed to 18% increase in nonischemic rabbit HF (Figure 3D). These results suggest a differential remodeling between ischemic versus nonischemic HF in the two species. However, the significant correlation between  $I_{Kr}$  and  $I_{NaL}$  was absent in both HF models.

## Discussion

### Contribution of $I_{Kr}$ and $I_{NaL}$ to AP morphology

Imbalance between depolarizing and repolarizing currents results in abnormal AP morphology and APD changes in cardiac myocytes that manifests as altered QT interval on the electrocardiogram. Our data demonstrate that  $I_{Kr}$  and  $I_{NaL}$  are not only major determinants of APD, but they counterbalance each other during the physiological AP of rabbit ventricular cardiomyocytes (Figures 2 and 4). Importantly,  $I_{Kr}$  and  $I_{NaL}$  peak densities and peak charges measured in the same cell significantly correlated with each other (but not with the baseline APD) both in rabbit (Figure 2) and porcine cardiomyocytes (Figure 7) despite more than 2-fold cell-to-cell variability in their magnitudes in control. Moreover, the significant statistical correlation between  $I_{Kr}$  and  $I_{NaL}$  was still present using a canonical AP-clamp (i.e., same voltage profile; Figure 3) in line with the recently demonstrated coupled transcription and functional expression of  $Na_v1.5$  and hERG.<sup>26</sup> Furthermore, if one of these currents is either reduced or enhanced leading to impaired AP repolarization, compensatory changes in the other current – dictated by the altered APD and plateau voltages – will affect the outcome on APD<sub>90</sub> and repolarization stability (Figure 2). The counterbalance between  $I_{Kr}$  and  $I_{NaL}$  on AP repolarization may have significant clinical implications and the  $I_{Kr}/I_{NaL}$  balance may represent an important antiarrhythmic target.

$I_{Kr}$  is considered a major repolarizing current affecting APD and repolarization stability<sup>27</sup> in ventricular cardiomyocytes of larger mammals including human.<sup>2</sup> However, the strong statistical correlation between the net charges of  $I_{Kr}$  and  $I_{NaL}$  (in rabbits, Figure 2L; in pigs, Figure 7F) as well as the opposing impact of these currents on APD (Figure 4) and repolarization stability (Figure 5) are striking yet not completely unexpected findings, as previously reviewed.<sup>9</sup> Most previous studies measured a smaller  $I_{NaL}$  of  $\approx -0.3$  pA/pF at  $-20$  mV in both human,<sup>28</sup> canine,<sup>29</sup> and rabbit<sup>30</sup> ventricular myocytes under conventional square voltage pulses and in the presence of strong intracellular  $Ca^{2+}$  buffers to eliminate  $[Ca^{2+}]_i$  transient. However, CaMKII has been previously demonstrated to significantly upregulate  $I_{NaL}$ .<sup>29, 31, 32</sup> This physiological CaMKII-dependent upregulation of  $I_{NaL}$  might have been missed in earlier biophysical studies, but our more physiological conditions to measure  $I_{NaL}$  (with preserved  $Ca^{2+}$  transient and CaMKII activation under the AP) was able to reveal the true magnitude of the current.<sup>5, 33</sup> We found a smaller  $I_{NaL}$  peak density under self AP-clamp

in porcine rabbit ventricular myocytes (Figure 7) than in rabbit; however,  $I_{NaL}$  net charge was similar to that in rabbit because of the longer APD in pigs. Previous studies used tetrodotoxin (TTX) almost exclusively to measure  $I_{NaL}$  raising a dilemma. Cardiac  $Na^+$  channels (predominantly  $Na_v1.5$ ) are insensitive to TTX with an  $IC_{50}$  of 1 to 2  $\mu\text{mol/L}$ .<sup>34,35</sup> Thus higher concentrations of TTX (10 to 30  $\mu\text{mol/L}$ ) are needed to achieve complete  $Na^+$  channel inhibition in cardiomyocytes which may have off-target effect on L-type  $Ca^{2+}$  channels.<sup>36</sup> The other option is to use lower concentrations of TTX, but in this case the magnitude of  $I_{NaL}$  will be underestimated. Hence we used GS-967 which does not have such off-target effect and exhibits higher selectivity for  $I_{NaL}$  over  $I_{NaT}$ .<sup>30,33</sup>

The positive rate-dependence of GS-967 effect on  $APD_{90}$  (Figure 6) is a conflicting finding with previous reports showing smaller  $I_{NaL}$  at higher frequency stimulation.<sup>11</sup> Possible explanations may include the state-dependent binding of GS-967 to the  $Na^+$  channels<sup>37</sup> and significant CaMKII-dependent modulation of  $I_{NaL}$  at rapid pacing rates.<sup>33</sup> Interestingly, ranolazine also caused more pronounced QT shortening at rapid heart rates than during bradycardia in LQT3 patients.<sup>14</sup> The underlying mechanisms require further investigation. On the contrary,  $I_{Kr}$  inhibition showed a well-known reverse-rate dependent effect on  $APD_{90}$  as it followed the frequency-dependent changes in baseline  $APD_{90}$  (Figure 6), which is characteristic to the myocardium.<sup>38</sup>

Our AP-clamp data revealed that  $I_{NaL}$  activates earlier than  $I_{Kr}$  during the AP (Figure 2), thus a significant  $I_{NaL}$  can be measured already under the mid-plateau phase of the AP where small depolarizing and repolarizing currents delicately balance each other.<sup>6</sup> This feature can be accountable for the strong influence of  $I_{NaL}$  inhibition on  $APD_{90}$  and repolarization stability despite the small  $I_{NaL}$  amplitude in accordance with modeling data.<sup>7,8</sup> Moreover,  $I_{NaL}$  inhibition may also decrease intracellular  $Na^+$  and  $Ca^{2+}$  load that has been shown to occur under a prolonged APD,<sup>39</sup> during tachypacing-induced APD alternans<sup>40</sup> and in HF.<sup>41</sup>

Remodeling of  $I_{Kr}$  and  $I_{NaL}$  is frequently reported in HF,<sup>18,22,42</sup> which introduces a shift in  $I_{Kr}/I_{NaL}$  balance and significantly contribute to the increased arrhythmia risk. We found enhanced  $I_{NaL}$  in both rabbit nonischemic HF (Figure 3) and porcine ischemic HF (Figure 7); however,  $I_{NaL}$  upregulation was more pronounced in the nonischemic model.  $I_{Kr}$  was slightly altered in HF in line with previous studies.<sup>42</sup>  $I_{Kr}$  was downregulated in porcine ischemic HF (Figure 7), whereas a  $Ca^{2+}$ -dependent  $I_{Kr}$  upregulation was found in rabbit nonischemic HF (Figure 3). The mechanism of differential ion channel remodeling in ischemic versus nonischemic HF has not been elucidated yet.

### Clinical and preclinical findings supporting the importance of $I_{Kr}/I_{NaL}$ balance

Targeting the balance between  $I_{Kr}$  and  $I_{NaL}$  may have significant therapeutic potential in QT abnormalities caused by either genetic or acquired conditions affecting these ion channels. Accordingly, mexiletine treatment was found to be effective in reducing the dispersion of repolarization and preventing torsades de pointes ventricular tachycardia in both LQT2 and LQT3 models.<sup>12</sup> Similarly,  $I_{Kr}$  inhibition in short QT syndrome represents a potential therapeutic approach to normalize the duration of repolarization; however, the mutant channels may express differential sensitivity for inhibitors.<sup>43</sup> Importantly, several

antiarrhythmic drugs successfully used in clinic including amiodarone,<sup>44</sup> ranolazine,<sup>45</sup> flecainide and quinidine<sup>46</sup> inhibit both  $I_{Kr}$  and  $I_{NaL}$ . These drugs, previously thought to have off-target effects, may finetune the ratio between  $I_{Kr}/I_{NaL}$  block to exert antiarrhythmic effects. Understanding the importance of the counterbalancing effect of  $I_{Kr}$  and  $I_{NaL}$ , the ratio between  $I_{Kr}/I_{NaL}$  block need to be considered when choosing an appropriate drug to treat a specific clinical condition.

Our experimental results confirm the predictions of a quantitative computational model<sup>47</sup> showing that selective  $I_{NaL}$  inhibition has beneficial effects on several factors considered to be proarrhythmic in LQT as  $I_{NaL}$  inhibition suppressed APD prolongation (Figure 4), beat-to-beat repolarization instability (Figure 5) and APD alternans (Figure 6). These results are in accordance with the effective suppression of re-entrant and multifocal ventricular fibrillation by  $I_{NaL}$  inhibition.<sup>48</sup>

When the repolarization is compromised, it may impair  $[Na^+]_i$  and  $[Ca^{2+}]_i$  homeostasis leading to CaMKII activation and generation of reactive oxygen species, which then feedback on ion channels forming a vicious cycle.<sup>49,50</sup> It is particularly true for HF, which is characterized by reduced repolarization reserve, increased  $I_{NaL}$  and enhanced CaMKII-mediated SR  $Ca^{2+}$  leak, all of them significantly increase the risk of arrhythmias.<sup>18,21,22,25</sup> Therefore, breaking the detrimental positive feedback loop can have a large benefit especially in HF, but also in LQT. Accordingly, inhibitors of CaMKII and  $I_{NaL}$  were found advantageous in numerous preclinical studies, but the confirmation of this concept in clinical trials is still yet to come.<sup>10,50</sup>

### Clinical and preclinical findings limiting the importance of $I_{Kr}/I_{NaL}$ balance

Despite the strong coupling between  $I_{Kr}$  and  $I_{NaL}$  under physiological AP repolarization, we found the timing of these ionic currents during AP shows major differences. Our AP-clamp data indicate that  $I_{NaL}$  has more influence on mid-plateau potentials and  $I_{Kr}$  predominantly affects phase 3 repolarization rate (Figures 2 and 4). These differences may explain (1) the differential susceptibility to EAD formation in LQT2 and LQT3 models<sup>51,52</sup> and (2) the large differences in the clinical manifestations of LQT2 and LQT3.<sup>1,2</sup> Moreover, the magnitude of both  $I_{Kr}$  and  $I_{NaL}$  significantly varies across species and exhibits significant spatial difference between cardiac regions.<sup>10,53</sup>

$I_{Kr}/I_{NaL}$  balance may also vary at different heart rates.  $I_{Kr}$  has activation and deactivation time constants of ~100 to 200 ms and more rapid kinetics of inactivation and recovery from inactivation in rabbit and human ventricular cardiomyocytes, thus  $I_{Kr}$  may accumulate at rapid heart rates.<sup>53</sup>  $I_{NaL}$  inactivation time constant is ~600 ms and  $I_{NaL}$  was reported to decrease with shorter diastolic intervals.<sup>11</sup> LQT2 and LQT3 (but not LQT1) patients have generally higher risk of arrhythmias at slower heart rates; however, in carriers of specific mutations (eg, S1904L in SCN5A encoding  $Na_v1.5$ ) arrhythmia is more frequent at rapid heart rates.<sup>2</sup> Moreover,  $I_{NaL}$  was shown to be involved in reverse-rate dependence of  $I_{Kr}$  inhibition on APD<sup>11</sup> that can be proarrhythmic in patients treated with  $I_{Kr}$  inhibiting drugs or carrying LQT2 mutations.

Nonetheless, cardiac arrhythmias are frequently triggered by increased sympathetic activity in LQT patients,<sup>1,2</sup> which may shift the balance between inward and outward ionic currents including not only  $I_{CaL}$  and  $I_{Ks}$ ,<sup>54,55</sup> but also  $I_{NaL}$  and  $I_{Kr}$ .<sup>56</sup>  $\beta$ -adrenergic agonist isoproterenol significantly enhances  $I_{NaL}$  via both protein kinase A and CaMKII-dependent mechanisms.<sup>33</sup> On the contrary  $I_{Kr}$  response to isoproterenol is variable between preparations and may involve regulation via protein kinase A and protein kinase C.<sup>18</sup> Although similar  $EC_{50}$  values of isoproterenol ( $\sim 10$  nmol/L) was found to activate  $I_{NaL}$  and  $I_{Kr}$ , the maximal responses were largely different (2.4- versus 1.1- to 1.3-fold increases for  $I_{NaL}$  and  $I_{Kr}$ , respectively),<sup>18,22,57</sup> indicating that  $I_{Kr}/I_{NaL}$  balance is shifted during  $\beta$ -adrenergic stimulation. This may partially explain why  $\beta$  blockers are still the preferred treatment in LQT patients as they significantly reduce the risk of arrhythmias.<sup>2</sup>

## Perspectives

It has been previously shown that  $Na_v1.5$  and  $K_{ir2.1}$  exhibit coordinated expression and they traffic together from trans-Golgi to sarcolemma to control excitability,<sup>58</sup> whereas such coordination between  $Na_v1.5$  and hERG may control repolarization stability in the heart, suggested recently by the coupled transcription and correlation of  $Na_v1.5$  and hERG surface expression levels.<sup>26</sup> The quantitative correlation we see between mean  $I_{Kr}$  and  $I_{NaL}$  during the AP could reflect this type of transcriptional co-regulation, but may be, in part, a manifestation of inherent voltage-dependent feedback between the channels during AP plateau voltages. However, the remarkable  $I_{NaL}$ - $I_{Kr}$  correlation within individual cells (where cells with the same APD can have in parallel much higher  $I_{NaL}$  and  $I_{Kr}$ ) makes the transcriptional co-regulation an attractive hypothesis for future work. Future studies are needed to reveal the exact contribution of  $I_{NaL}$  and  $I_{Kr}$  to  $Na^+$  and  $Ca^{2+}$  homeostasis under pathological conditions affecting AP repolarization because  $Ca^{2+}$  handling abnormalities further increase repolarization instability<sup>59,60</sup> and trigger arrhythmias in the intact heart.<sup>61</sup> Patient-specific human-induced pluripotent stem cell-derived cardiomyocytes can also provide important information on the different LQT phenotypes and their pharmacological modulation.<sup>62</sup> Further in vivo arrhythmia tests in large animal LQT, SQT and HF models which exhibit human-like repolarization reserve<sup>63</sup> are necessary to assess the therapeutic potential of targeting the  $I_{Kr}/I_{NaL}$  balance.

## Supplementary Material

Refer to Web version on PubMed Central for supplementary material.

## Acknowledgments

We thank Zhong Jian, Rafael Shimkunas, Mark Jaradeh, Logan R.J. Bailey, Johanna M. Borst, Benjamin W. Van, Maura Ferrero, and Julie Bossuyt for their help in animal care, cell isolation and laboratory tasks. We thank William T. Ferrier, Linda Talken, Lynette M. Mendoza, and Kenneth S. Ginsburg for their help in surgical procedures and echocardiographic follow-up of heart failure rabbits. We also thank Leigh G. Griffiths, Kristin N. Grimsrud, Claus S. Sondergaard, and W. Douglas Boyd for their help in surgical procedures and echocardiographic follow-up of heart failure pigs.

**Sources of Funding:** This work was supported by grants from the National Institute of Health R01-HL090880 (LTI and YCI), R01-HL123526 (YCI), R01-HL141460 (YCI), P01-HL141084 (DMB), R01-HL030077 (DMB) and R01-HL142282 (DMB); the American Heart Association 14GRNT20510041 (YCI); and the Hungarian Scientific Research Fund OTKA101196 (TB).

## Non-standard Abbreviations and Acronyms:

<b>APD</b>	Action potential duration
<b>ATX-II</b>	Sea anemone toxin II
<b>BrS</b>	Brugada syndrome
<b>CaMKII</b>	Ca <sup>2+</sup> /calmodulin-dependent protein kinase II
<b>-dV/dt<sub>max</sub></b>	Maximal rate of repolarization
<b>I<sub>Kr</sub></b>	Rapid delayed rectifier K <sup>+</sup> current
<b>I<sub>NaL</sub></b>	Late Na <sup>+</sup> current
<b>I<sub>NaT</sub></b>	Transient Na <sup>+</sup> current
<b>LQT</b>	Long QT syndrome
<b>SQT</b>	Short QT syndrome
<b>STV</b>	Short-term variability of APD
<b>TTX</b>	Tetrodotoxin

## References

1. Morita H, Wu J, Zipes DP. The QT syndromes: long and short. *Lancet*. 2008;372:750–763. [PubMed: 18761222]
2. Bohnen MS, Peng G, Robey SH, Terrenoire C, Iyer V, Sampson KJ, Kass RS. Molecular Pathophysiology of Congenital Long QT Syndrome. *Physiol Rev*. 2017;97:89–134. [PubMed: 27807201]
3. Antzelevitch C, Brugada P, Borggreffe M, Brugada J, Brugada R, Corrado D, Gussak I, LeMarec H, Nademanee K, Perez Riera AR, et al. Brugada syndrome: report of the second consensus conference: endorsed by the Heart Rhythm Society and the European Heart Rhythm Association. *Circulation*. 2005;111:659–670. [PubMed: 15655131]
4. Brugada R, Hong K, Dumaine R, Cordeiro J, Gaita F, Borggreffe M, Menendez TM, Brugada J, Pollevick GD, Wolpert C, et al. Sudden death associated with short-QT syndrome linked to mutations in HERG. *Circulation*. 2004;109:30–35. [PubMed: 14676148]
5. Horvath B, Banyasz T, Jian Z, Hegyí B, Kistamas K, Nanasi PP, Izu LT, Chen-Izu Y. Dynamics of the late Na(+) current during cardiac action potential and its contribution to afterdepolarizations. *J Mol Cell Cardiol*. 2013;64:59–68. [PubMed: 24012538]
6. Hegyí B, Bossuyt J, Griffiths LG, Shimkunas R, Coulibaly Z, Jian Z, Grimsrud KN, Sondergaard CS, Ginsburg KS, Chiamvimonvat N, et al. Complex electrophysiological remodeling in postinfarction ischemic heart failure. *Proc Natl Acad Sci U S A*. 2018;115:E3036–E3044. [PubMed: 29531045]
7. Noble D, Noble PJ. Late sodium current in the pathophysiology of cardiovascular disease: consequences of sodium-calcium overload. *Heart*. 2006;92 Suppl 4:iv1–iv5. [PubMed: 16775091]
8. Yang PC, Song Y, Giles WR, Horvath B, Chen-Izu Y, Belardinelli L, Rajamani S, Clancy CE. A computational modelling approach combined with cellular electrophysiology data provides insights into the therapeutic benefit of targeting the late Na<sup>+</sup> current. *J Physiol*. 2015;593:1429–1442. [PubMed: 25545172]
9. Zaza A, Rocchetti M. The late Na<sup>+</sup> current--origin and pathophysiological relevance. *Cardiovasc Drugs Ther*. 2013;27:61–68. [PubMed: 23274937]

10. Belardinelli L, Giles WR, Rajamani S, Karagueuzian HS, Shryock JC. Cardiac late Na<sup>+</sup> current: proarrhythmic effects, roles in long QT syndromes, and pathological relationship to CaMKII and oxidative stress. *Heart Rhythm*. 2015;12:440–448. [PubMed: 25460862]
11. Wu L, Ma J, Li H, Wang C, Grandi E, Zhang P, Luo A, Bers DM, Shryock JC, Belardinelli L. Late sodium current contributes to the reverse rate-dependent effect of IKr inhibition on ventricular repolarization. *Circulation*. 2011;123:1713–1720. [PubMed: 21482963]
12. Shimizu W, Antzelevitch C. Sodium channel block with mexiletine is effective in reducing dispersion of repolarization and preventing torsade des pointes in LQT2 and LQT3 models of the long-QT syndrome. *Circulation*. 1997;96:2038–2047. [PubMed: 9323097]
13. Bos JM, Crotti L, Rohatgi RK, Castelletti S, Dagradi F, Schwartz PJ, Ackerman MJ. Mexiletine Shortens the QT Interval in Patients With Potassium Channel-Mediated Type 2 Long QT Syndrome. *Circ Arrhythm Electrophysiol*. 2019;12:e007280. [PubMed: 31006312]
14. Chorin E, Hu D, Antzelevitch C, Hochstadt A, Belardinelli L, Zeltser D, Barajas-Martinez H, Rozovski U, Rosso R, Adler A, et al. Ranolazine for Congenital Long-QT Syndrome Type III: Experimental and Long-Term Clinical Data. *Circ Arrhythm Electrophysiol*. 2016;9.
15. Giustetto C, Schimpf R, Mazzanti A, Scrocco C, Maury P, Anttonen O, Probst V, Blanc JJ, Sbragia P, Dalmasso P, et al. Long-term follow-up of patients with short QT syndrome. *J Am Coll Cardiol*. 2011;58:587–595. [PubMed: 21798421]
16. Andorin A, Gourraud JB, Mansourati J, Fouchard S, le Marec H, Maury P, Mabo P, Hermida JS, Deharo JC, Delasalle B, et al. The QUIDAM study: Hydroquinidine therapy for the management of Brugada syndrome patients at high arrhythmic risk. *Heart Rhythm*. 2017;14:1147–1154. [PubMed: 28411139]
17. Chen-Izu Y, Izu LT, Hegyí B, Bányász T. Recording of Ionic Currents Under Physiological Conditions: Action Potential-Clamp and ‘Onion-Peeling’ Techniques In: Jue T, ed. *Modern Tools of Biophysics* New York, NY: Springer New York; 2017: 31–48.
18. Hegyí B, Bossuyt J, Ginsburg KS, Mendoza LM, Talken L, Ferrier WT, Pogwizd SM, Izu LT, Chen-Izu Y, Bers DM. Altered Repolarization Reserve in Failing Rabbit Ventricular Myocytes: Calcium and  $\beta$ -Adrenergic Effects on Delayed- and Inward-Rectifier Potassium Currents. *Circ Arrhythm Electrophysiol*. 2018;11:e005852. [PubMed: 29437761]
19. Piccirillo G, Magri D, Matera S, Magnanti M, Torrini A, Pasquazzi E, Schifano E, Velitti S, Marigliano V, Quaglione R, et al. QT variability strongly predicts sudden cardiac death in asymptomatic subjects with mild or moderate left ventricular systolic dysfunction: a prospective study. *Eur Heart J*. 2007;28:1344–1350. [PubMed: 17101636]
20. Hegyí B, Chen-Izu Y, Izu LT, Banyasz T. Altered K<sup>+</sup> current profiles underlie cardiac action potential shortening in hyperkalemia and beta-adrenergic stimulation. *Can J Physiol Pharmacol*. 2019;97:773–780. [PubMed: 31091413]
21. Pogwizd SM, Schlotthauer K, Li L, Yuan W, Bers DM. Arrhythmogenesis and contractile dysfunction in heart failure: Roles of sodium-calcium exchange, inward rectifier potassium current, and residual beta-adrenergic responsiveness. *Circ Res*. 2001;88:1159–1167. [PubMed: 11397782]
22. Hegyí B, Morotti S, Liu C, Ginsburg KS, Bossuyt J, Belardinelli L, Izu LT, Chen-Izu Y, Banyasz T, Grandi E, et al. Enhanced Depolarization Drive in Failing Rabbit Ventricular Myocytes. *Circ Arrhythm Electrophysiol*. 2019;12:e007061. [PubMed: 30879336]
23. Szentandrassy N, Kistamas K, Hegyí B, Horvath B, Ruzsnavszky F, Vaczi K, Magyar J, Banyasz T, Varro A, Nanasi PP. Contribution of ion currents to beat-to-beat variability of action potential duration in canine ventricular myocytes. *Pflugers Arch*. 2015;467:1431–1443. [PubMed: 25081243]
24. Hegyí B, Horvath B, Vaczi K, Gonczi M, Kistamas K, Ruzsnavszky F, Veress R, Izu LT, Chen-Izu Y, Banyasz T, et al. Ca<sup>2+</sup>-activated Cl<sup>-</sup> current is antiarrhythmic by reducing both spatial and temporal heterogeneity of cardiac repolarization. *J Mol Cell Cardiol*. 2017;109:27–37. [PubMed: 28668303]
25. Ai X, Curran JW, Shannon TR, Bers DM, Pogwizd SM. Ca<sup>2+</sup>/calmodulin-dependent protein kinase modulates cardiac ryanodine receptor phosphorylation and sarcoplasmic reticulum Ca<sup>2+</sup> leak in heart failure. *Circ Res*. 2005;97:1314–1322. [PubMed: 16269653]

26. Eichel CA, Rios-Perez EB, Liu F, Jameson MB, Jones DK, Knickelbine JJ, Robertson GA. A microtranslatome coordinately regulates sodium and potassium currents in the human heart. *eLife*. 2019;8: e52654. doi: 10.7554/eLife.52654. [PubMed: 31670657]
27. Altomare C, Bartolucci C, Sala L, Bernardi J, Mostacciolo G, Rocchetti M, Severi S, Zaza A. IKr Impact on Repolarization and Its Variability Assessed by Dynamic Clamp. *Circ Arrhythm Electrophysiol*. 2015;8:1265–1275. [PubMed: 26105569]
28. Maltsev VA, Sabbah HN, Higgins RS, Silverman N, Lesch M, Undrovinas AI. Novel, ultraslow inactivating sodium current in human ventricular cardiomyocytes. *Circulation*. 1998;98:2545–2552. [PubMed: 9843461]
29. Maltsev VA, Reznikov V, Undrovinas NA, Sabbah HN, Undrovinas A. Modulation of late sodium current by Ca<sup>2+</sup>, calmodulin, and CaMKII in normal and failing dog cardiomyocytes: similarities and differences. *Am J Physiol Heart Circ Physiol*. 2008;294:H1597–H1608. [PubMed: 18203851]
30. Belardinelli L, Liu G, Smith-Maxwell C, Wang WQ, El-Bizri N, Hirakawa R, Karpinski S, Li CH, Hu L, Li XJ, et al. A novel, potent, and selective inhibitor of cardiac late sodium current suppresses experimental arrhythmias. *J Pharmacol Exp Ther*. 2013;344:23–32. [PubMed: 23010360]
31. Wagner S, Dybkova N, Rasenack EC, Jacobshagen C, Fabritz L, Kirchhof P, Maier SK, Zhang T, Hasenfuss G, Brown JH, et al. Ca<sup>2+</sup>/calmodulin-dependent protein kinase II regulates cardiac Na<sup>+</sup> channels. *J Clin Invest*. 2006;116:3127–3138. [PubMed: 17124532]
32. Glynn P, Musa H, Wu X, Unudurthi SD, Little S, Qian L, Wright PJ, Radwanski PB, Gyorke S, Mohler PJ, et al. Voltage-Gated Sodium Channel Phosphorylation at Ser571 Regulates Late Current, Arrhythmia, and Cardiac Function In Vivo. *Circulation*. 2015;132:567–577. [PubMed: 26187182]
33. Hegyí B, Banyasz T, Izu LT, Belardinelli L, Bers DM, Chen-Izu Y.  $\beta$ -adrenergic regulation of late Na<sup>+</sup> current during cardiac action potential is mediated by both PKA and CaMKII. *J Mol Cell Cardiol*. 2018;123:168–179. [PubMed: 30240676]
34. Hegyí B, Komaromi I, Nanasi PP, Szentandrassy N. Selectivity Problems with Drugs Acting on Cardiac Na<sup>+</sup> and Ca<sup>2+</sup> Channels. *Curr Med Chem*. 2013;20:2552–2571. [PubMed: 23597201]
35. Haufe V, Cordeiro JM, Zimmer T, Wu YS, Schiccitano S, Benndorf K, Dumaine R. Contribution of neuronal sodium channels to the cardiac fast sodium current I<sub>Na</sub> is greater in dog heart Purkinje fibers than in ventricles. *Cardiovasc Res*. 2005;65:117–127. [PubMed: 15621039]
36. Hegyí B, Barandi L, Komaromi I, Papp F, Horvath B, Magyar J, Banyasz T, Krasznai Z, Szentandrassy N, Nanasi PP. Tetrodotoxin blocks L-type Ca<sup>2+</sup> channels in canine ventricular cardiomyocytes. *Pflugers Arch*. 2012;464:167–174. [PubMed: 22615072]
37. Koltun DO, Parkhill EQ, Elzein E, Kobayashi T, Notte GT, Kalla R, Jiang RH, Li X, Perry TD, Avila B, et al. Discovery of triazolopyridine GS-458967, a late sodium current inhibitor (Late I<sub>Na</sub>) of the cardiac NaV 1.5 channel with improved efficacy and potency relative to ranolazine. *Bioorg Med Chem Lett*. 2016;26:3202–3206. [PubMed: 27080178]
38. Barandi L, Virag L, Jost N, Horvath Z, Koncz I, Papp R, Harmati G, Horvath B, Szentandrassy N, Banyasz T, et al. Reverse rate-dependent changes are determined by baseline action potential duration in mammalian and human ventricular preparations. *Basic Res Cardiol*. 2010;105:315–323. [PubMed: 20127488]
39. Kornyejev D, El-Bizri N, Hirakawa R, Nguyen S, Viatchenko-Karpinski S, Yao L, Rajamani S, Belardinelli L. Contribution of the late sodium current to intracellular sodium and calcium overload in rabbit ventricular myocytes treated by anemone toxin. *Am J Physiol Heart Circ Physiol*. 2016;310:H426–H435. [PubMed: 26637557]
40. Wasserstrom JA, Sharma R, O'Toole MJ, Zheng J, Kelly JE, Shryock J, Belardinelli L, Aistrup GL. Ranolazine antagonizes the effects of increased late sodium current on intracellular calcium cycling in rat isolated intact heart. *J Pharmacol Exp Ther*. 2009;331:382–391. [PubMed: 19675298]
41. Ke HY, Yang HY, Francis AJ, Collins TP, Surendran H, Alvarez-Laviada A, Firth JM, MacLeod KT. Changes in cellular Ca<sup>2+</sup> and Na<sup>+</sup> regulation during the progression towards heart failure in the guinea pig. *J Physiol*. 2019. doi: 10.1113/JP277038.

42. Nattel S, Maguy A, Le Bouter S, Yeh YH. Arrhythmogenic ion-channel remodeling in the heart: heart failure, myocardial infarction, and atrial fibrillation. *Physiol Rev.* 2007;87:425–456. [PubMed: 17429037]
43. Gaita F, Giustetto C, Bianchi F, Schimpf R, Haissaguerre M, Calo L, Brugada R, Antzelevitch C, Borggrefe M, Wolpert C. Short QT syndrome: pharmacological treatment. *J Am Coll Cardiol.* 2004;43:1494–1499. [PubMed: 15093889]
44. Wu L, Rajamani S, Shryock JC, Li H, Ruskin J, Antzelevitch C, Belardinelli L. Augmentation of late sodium current unmasks the proarrhythmic effects of amiodarone. *Cardiovasc Res.* 2008;77:481–488. [PubMed: 18006430]
45. Antzelevitch C, Belardinelli L, Zygmunt AC, Burashnikov A, Di Diego JM, Fish JM, Cordeiro JM, Thomas G. Electrophysiological effects of ranolazine, a novel antianginal agent with antiarrhythmic properties. *Circulation.* 2004;110:904–910. [PubMed: 15302796]
46. Paul AA, Witchel HJ, Hancox JC. Inhibition of the current of heterologously expressed HERG potassium channels by flecainide and comparison with quinidine, propafenone and lignocaine. *Br J Pharmacol.* 2002;136:717–729. [PubMed: 12086981]
47. Yang PC, El-Bizri N, Romero L, Giles WR, Rajamani S, Belardinelli L, Clancy CE. A computational model predicts adjunctive pharmacotherapy for cardiac safety via selective inhibition of the late cardiac Na current. *J Mol Cell Cardiol.* 2016;99:151–161. [PubMed: 27545042]
48. Morita N, Lee JH, Xie Y, Sovari A, Qu Z, Weiss JN, Karagueuzian HS. Suppression of re-entrant and multifocal ventricular fibrillation by the late sodium current blocker ranolazine. *J Am Coll Cardiol.* 2011;57:366–375. [PubMed: 21232675]
49. Morotti S, Grandi E. Quantitative systems models illuminate arrhythmia mechanisms in heart failure: Role of the  $\text{Na}^+$ - $\text{Ca}^{2+}$ - $\text{Ca}^{2+}$ /calmodulin-dependent protein kinase II-reactive oxygen species feedback. *Wiley Interdiscip Rev Syst Biol Med.* 2019;11:e1434. [PubMed: 30015404]
50. Hegyí B, Bers DM, Bossuyt J. CaMKII signaling in heart diseases: Emerging role in diabetic cardiomyopathy. *J Mol Cell Cardiol.* 2019;127:246–259. [PubMed: 30633874]
51. Studenik CR, Zhou Z, January CT. Differences in action potential and early afterdepolarization properties in LQT2 and LQT3 models of long QT syndrome. *Br J Pharmacol.* 2001;132:85–92. [PubMed: 11156564]
52. Horvath B, Hegyí B, Kistamas K, Vaczi K, Banyasz T, Magyar J, Szentandrassy N, Nanasi PP. Cytosolic calcium changes affect the incidence of early afterdepolarizations in canine ventricular myocytes. *Can J Physiol Pharmacol.* 2015;93:527–534. [PubMed: 25928391]
53. Tseng GN. I(Kr): the hERG channel. *J Mol Cell Cardiol.* 2001;33:835–849. [PubMed: 11343409]
54. Xie Y, Grandi E, Puglisi JL, Sato D, Bers DM. beta-adrenergic stimulation activates early afterdepolarizations transiently via kinetic mismatch of PKA targets. *J Mol Cell Cardiol.* 2013;58:153–161. [PubMed: 23481579]
55. Ruzsnavszky F, Hegyí B, Kistamas K, Vaczi K, Horvath B, Szentandrassy N, Banyasz T, Nanasi PP, Magyar J. Asynchronous activation of calcium and potassium currents by isoproterenol in canine ventricular myocytes. *Naunyn Schmiedebergs Arch Pharmacol.* 2014;387:457–467. [PubMed: 24566722]
56. Szentmiklosi AJ, Szentandrassy N, Hegyí B, Horvath B, Magyar J, Banyasz T, Nanasi PP. Chemistry, physiology, and pharmacology of  $\beta$ -adrenergic mechanisms in the heart. Why are  $\beta$ -blocker antiarrhythmics superior? *Curr Pharm Des.* 2015;21:1030–1041. [PubMed: 25354180]
57. Szentandrassy N, Farkas V, Barandi L, Hegyí B, Ruzsnavszky F, Horvath B, Banyasz T, Magyar J, Marton I, Nanasi PP. Role of action potential configuration and the contribution of C(2)(+)a and K(+) currents to isoprenaline-induced changes in canine ventricular cells. *Br J Pharmacol.* 2012;167:599–611. [PubMed: 22563726]
58. Ponce-Balbuena D, Guerrero-Serna G, Valdivia CR, Caballero R, Diez-Guerra FJ, Jimenez-Vazquez EN, Ramirez RJ, Monteiro da Rocha A, Herron TJ, Campbell KF, et al. Cardiac Kir2.1 and NaV1.5 Channels Traffic Together to the Sarcolemma to Control Excitability. *Circ Res.* 2018;122:1501–1516. [PubMed: 29514831]
59. Johnson DM, Heijman J, Bode EF, Greensmith DJ, van der Linde H, Abi-Gerges N, Eisner DA, Trafford AW, Volders PG. Diastolic spontaneous calcium release from the sarcoplasmic reticulum

- increases beat-to-beat variability of repolarization in canine ventricular myocytes after beta-adrenergic stimulation. *Circ Res.* 2013;112:246–256. [PubMed: 23149594]
60. Kistamas K, Szentandrassy N, Hegyí B, Vaczi K, Ruzsnavszky F, Horvath B, Banyasz T, Nanasi PP, Magyar J. Changes in intracellular calcium concentration influence beat-to-beat variability of action potential duration in canine ventricular myocytes. *J Physiol Pharmacol.* 2015;66:73–81. [PubMed: 25716967]
  61. Kim JJ, Nemeç J, Li Q, Salama G. Synchronous systolic subcellular Ca<sup>2+</sup>-elevations underlie ventricular arrhythmia in drug-induced long QT type 2. *Circ Arrhythm Electrophysiol.* 2015;8:703–712. [PubMed: 25722252]
  62. Sala L, Gneçchi M, Schwartz PJ. Long QT Syndrome Modelling with Cardiomyocytes Derived from Human-induced Pluripotent Stem Cells. *Arrhythm Electrophysiol Rev.* 2019;8:105–110. [PubMed: 31114684]
  63. Baczko I, Jost N, Virag L, Bosze Z, Varro A. Rabbit models as tools for preclinical cardiac electrophysiological safety testing: Importance of repolarization reserve. *Prog Biophys Mol Biol.* 2016;121:157–168. [PubMed: 27208697]

**What is Known**

- Delayed rectifier  $K^+$  current ( $I_{Kr}$ , hERG channels) and late  $Na^+$  current ( $I_{NaL}$ , predominantly  $Na_v1.5$  channels) are significant contributors to ventricular action potential duration.
- Changes in  $I_{Kr}$  and  $I_{NaL}$  magnitudes cause repolarization abnormalities such as long and short QT syndromes with increased risk of cardiac arrhythmias.

**What the Study Adds**

- $I_{Kr}$  and  $I_{NaL}$  are in balance under the ventricular action potential and their magnitude significantly correlate among cardiomyocytes to control action potential duration and its temporal variability (beat-to-beat variations and tachypacing-induced alternans).
- Rebalancing  $I_{Kr}$  and  $I_{NaL}$  in disease (LQT2 and LQT3, short QT) can effectively normalize repolarization.
- $I_{Kr}$  and  $I_{NaL}$  are remodeled in ischemic and non-ischemic heart failure, their correlation is lost, and their balance is altered leading to impaired repolarization.

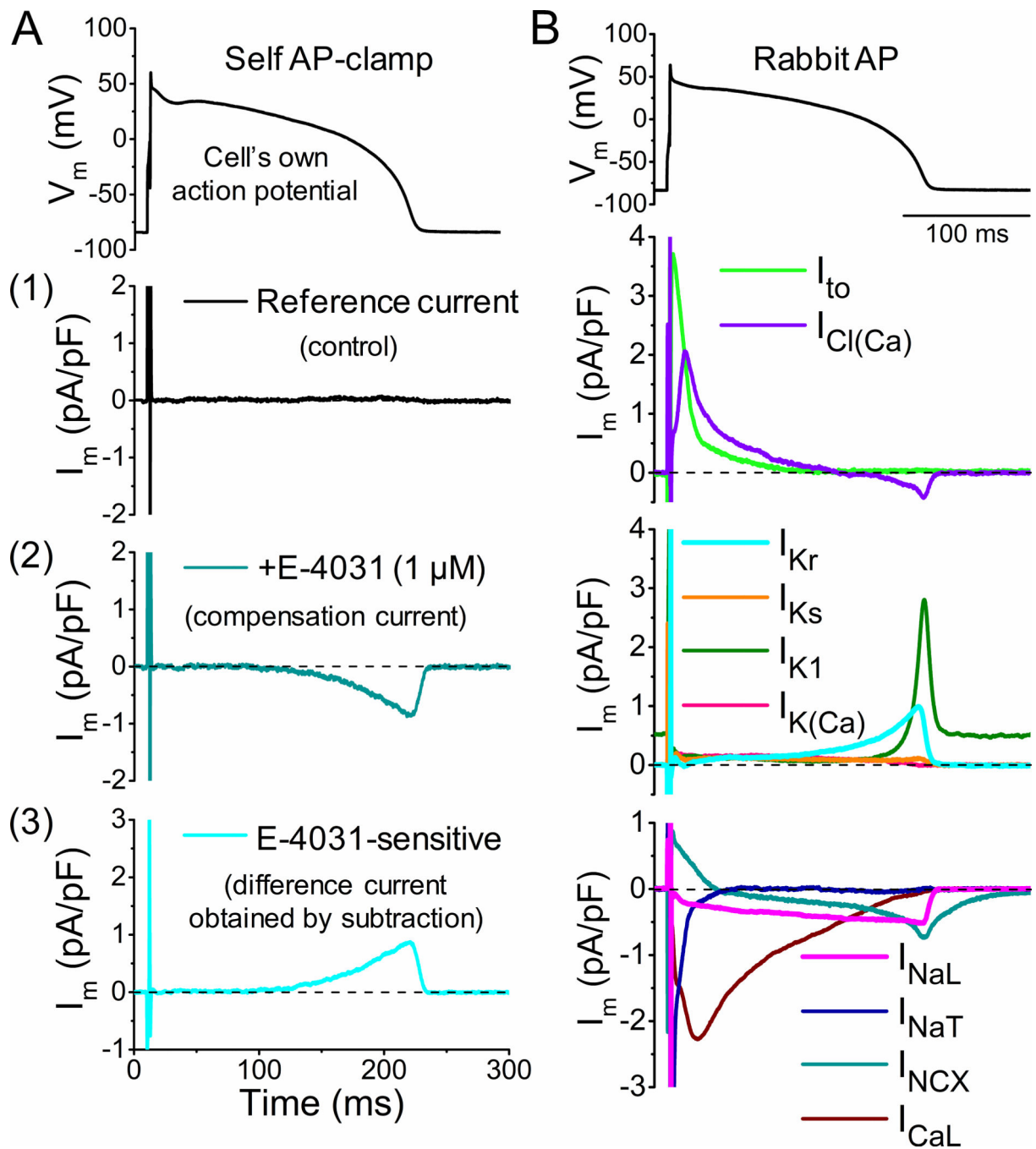


**Figure 1.**

Profile of the major ionic currents in rabbit ventricular cardiomyocytes under physiological action potential (AP)-clamp. **A**, Self AP-clamp technique to measure ionic currents under physiological AP. First, recording the cell's own steady-state AP, then using this AP as voltage command a pre-drug control or reference current (1) is obtained. Next, when a drug is applied (eg, E-4031), a compensation current (2) is recorded specific to the drug action. The drug-sensitive current (3) is obtained as the difference current (ie, subtracting the compensation current from the reference current). **B**, Representative traces of major ionic

currents in rabbit ventricular cardiomyocytes under physiological AP-clamp. Ionic currents were measured as drug-sensitive currents. Cells were paced at 2 Hz steady-state frequency at 36°C. Transient outward K<sup>+</sup> current (I<sub>to</sub>) and calcium-activated Cl<sup>-</sup> current (I<sub>Cl(Ca)</sub>) were measured as 4-aminopyridine and CaCCinh-A01-sensitive currents, respectively. Rapid delayed rectifier K<sup>+</sup> current (I<sub>Kr</sub>), slow delayed rectifier K<sup>+</sup> current (I<sub>Ks</sub>), inward rectifier K<sup>+</sup> current (I<sub>K1</sub>), and small conductance Ca<sup>2+</sup>-activated K<sup>+</sup> current (I<sub>K(Ca)</sub>) were measured as E-4031, HMR-1556, Ba<sup>2+</sup>, and apamin-sensitive currents, respectively. Late Na<sup>+</sup> current (I<sub>NaL</sub>), transient Na<sup>+</sup> current (I<sub>NaT</sub>), Na<sup>+</sup>/Ca<sup>2+</sup> exchange current (I<sub>NCX</sub>), and L-type Ca<sup>2+</sup> current (I<sub>CaL</sub>) were measured as GS-967, tetrodotoxin, ORM-10962, and nifedipine-sensitive currents, respectively. The peak of I<sub>NaT</sub> is out of range.

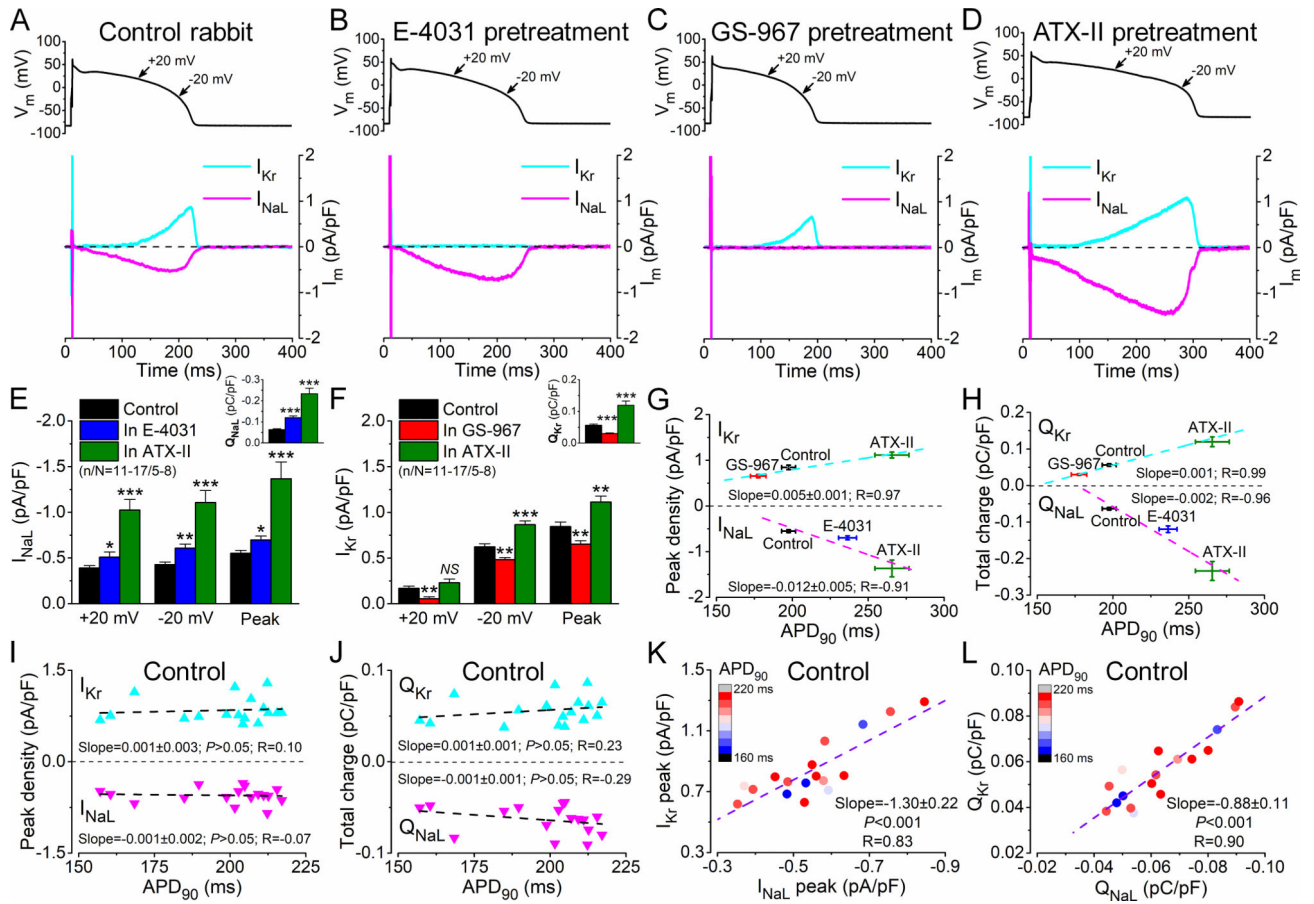


**Figure 2.** Correlation between  $I_{Kr}$  and  $I_{NaL}$  under self action potential (AP)-clamp. **A**,  $I_{Kr}$  and  $I_{NaL}$  under self AP-clamp in control rabbit ventricular cardiomyocytes.  $I_{NaL}$  and  $I_{Kr}$  were measured as 1  $\mu\text{mol/L}$  GS-967 and 1  $\mu\text{mol/L}$  E-4031-sensitive currents, respectively. Cells were paced at 2 Hz. **B**,  $I_{NaL}$  under a prolonged APD following  $I_{Kr}$  inhibition (E-4031 pretreatment). **C**,  $I_{Kr}$  under a shortened APD following  $I_{NaL}$  inhibition (GS-967 pretreatment). **D**,  $I_{NaL}$  and  $I_{Kr}$  under a prolonged APD following ATX-II (5 nmol/L) treatment to modulate  $\text{Na}^+$  channel inactivation. **E** and **F**,  $I_{Kr}$  and  $I_{NaL}$  densities in control, and following pretreatment with either E-4031, GS-967, or ATX-II. Inset shows the net charge carried by  $I_{NaL}$  and  $I_{Kr}$  under self AP-clamp. **G** and **H**, Correlation between APD and  $I_{Kr}$  or  $I_{NaL}$  peak densities and net charges measured in control and following pretreatment with either E-4031, GS-967, or ATX-II. **I** and **J**, No correlation between APD and  $I_{Kr}$  or  $I_{NaL}$  peak densities and net charges in individual control cells under self AP-clamp. **K** and **L**, Correlation between  $I_{Kr}$  and  $I_{NaL}$  peak densities and net charges obtained in each control cell under self AP-clamp. Dashed lines represent the fitted linear regression curves. Mean  $\pm$ SEM is shown.  $n/N$  refers to cells/animals measured in each group. ANOVA with Bonferroni posttest. *NS*, not significant ( $P>0.05$ ), \* $P<0.05$ , \*\* $P<0.01$ , \*\*\* $P<0.001$ .

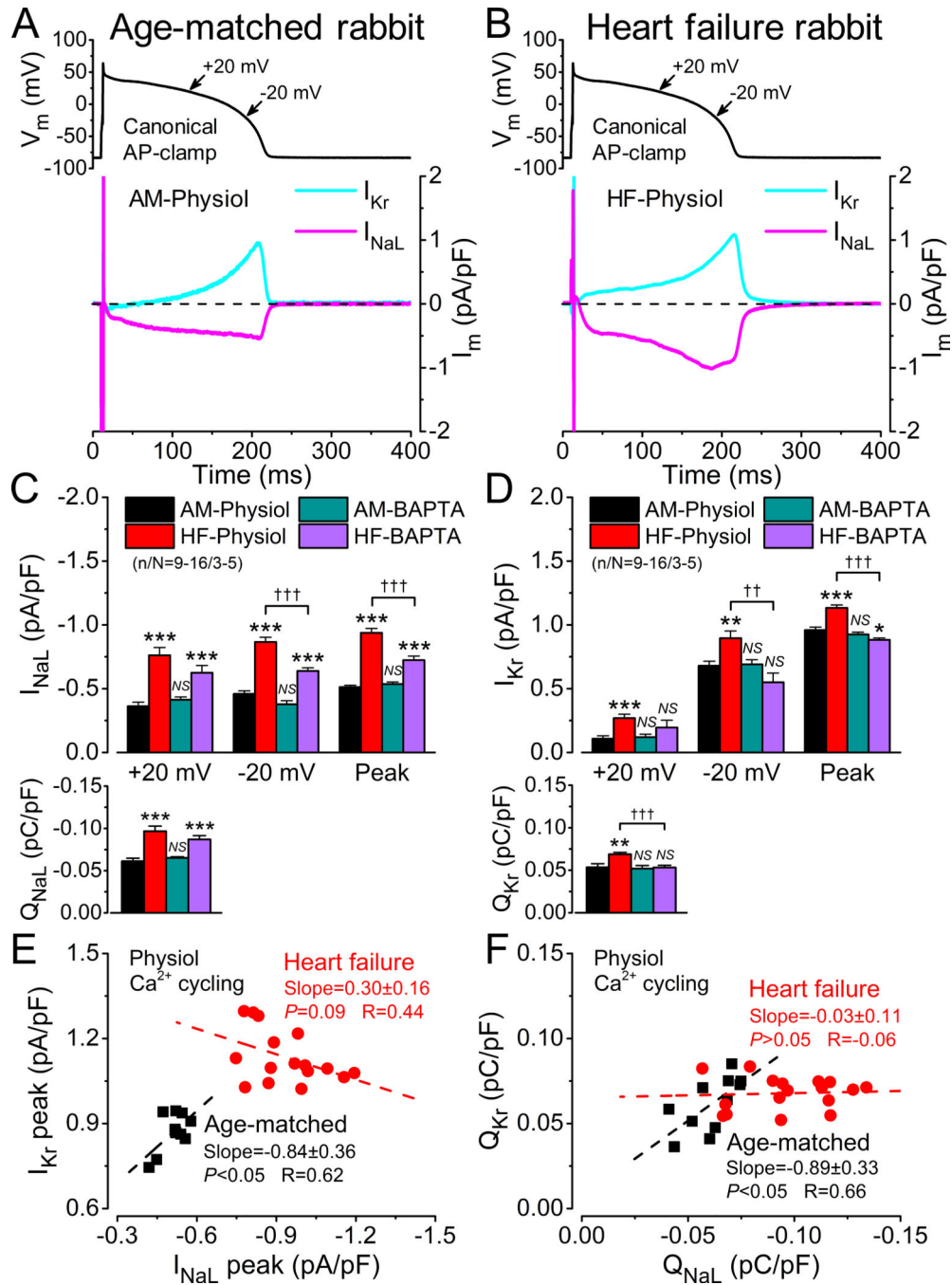


**Figure 3.** Heart failure shifts the balance between  $I_{Kr}$  and  $I_{NaL}$  in rabbit ventricular cardiomyocytes. **A** and **B**,  $I_{Kr}$  and  $I_{NaL}$  in rabbit heart failure (HF) and age-matched control (AM) under canonical AP-clamp.  $I_{NaL}$  and  $I_{Kr}$  were measured as 1  $\mu$ mol/L GS-967 and 1  $\mu$ mol/L E-4031-sensitive currents under AP-clamp, respectively. Cells were paced at 2 Hz using the same, prerecorded AP. **C** and **D**,  $I_{NaL}$  and  $I_{Kr}$  densities and net charges in HF and AM measured under physiological AP-clamp with preserved  $Ca^{2+}$  transient (Physiol) or in the presence of 10 mmol/L BAPTA in the pipette to eliminate  $Ca^{2+}$  transient (BAPTA). **E** and **F**,

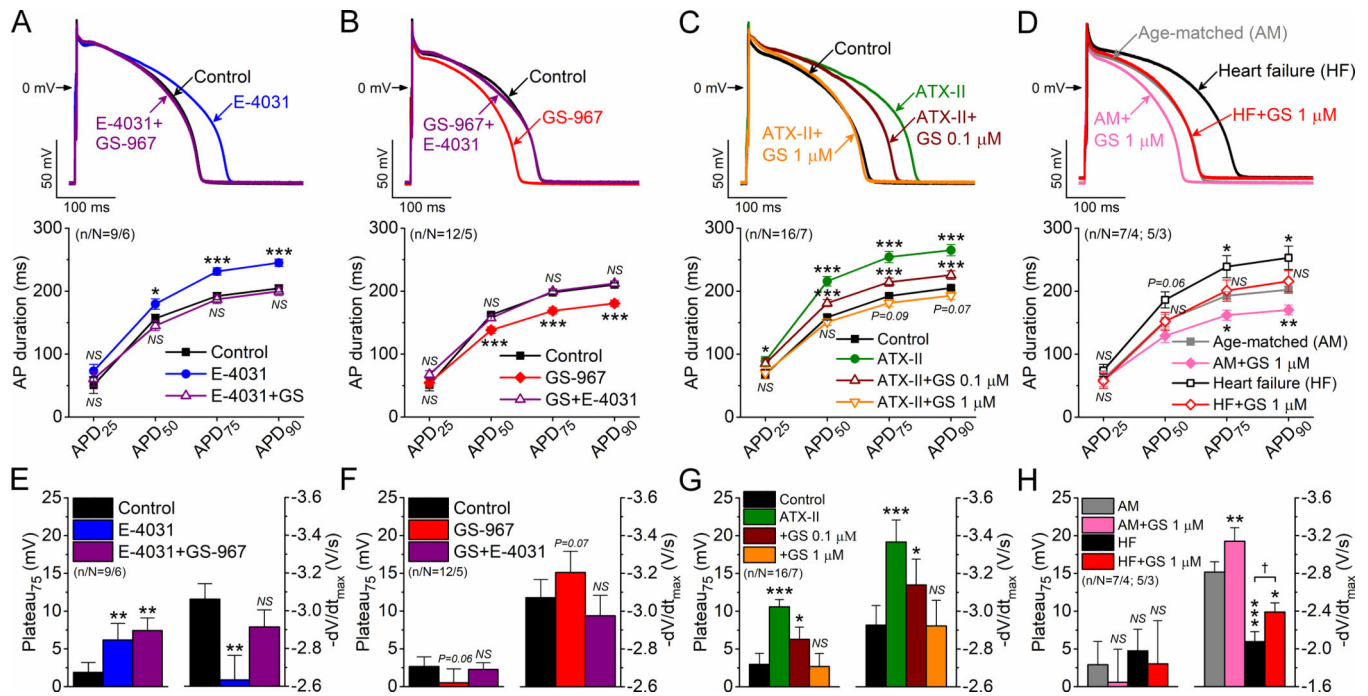
Correlation between  $I_{Kr}$  and  $I_{NaL}$  peak densities and net charges in HF and AM. Dashed lines represent the fitted linear regression curves. Mean $\pm$ SEM is shown.  $n/N$  refers to cells/animals measured in each group. ANOVA with Bonferroni posttest. *NS*, not significant ( $P>0.05$ ), \* $P<0.05$ , \*\* $P<0.01$ , \*\*\* $P<0.001$  versus AM-Physiol; †† $P<0.01$ , ††† $P<0.001$  versus HF-Physiol.

Author Manuscript

Author Manuscript

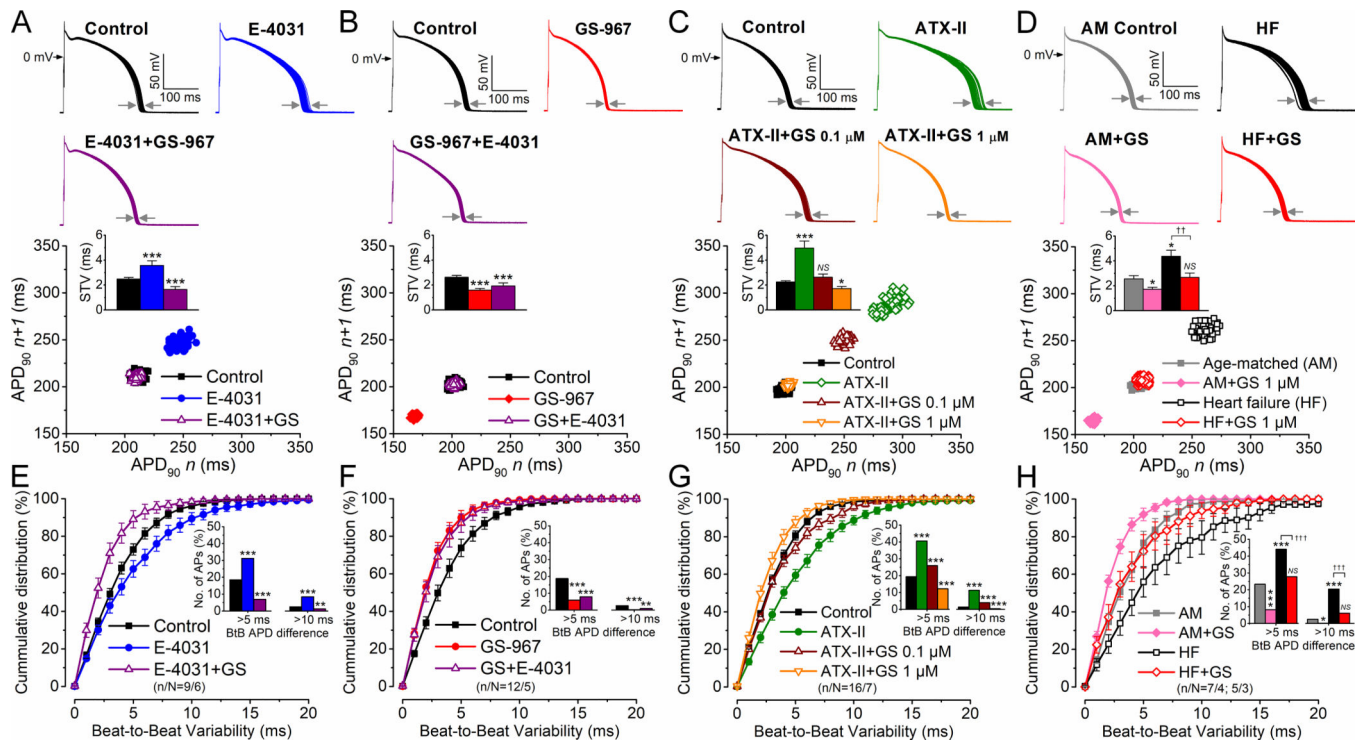
Author Manuscript

Author Manuscript



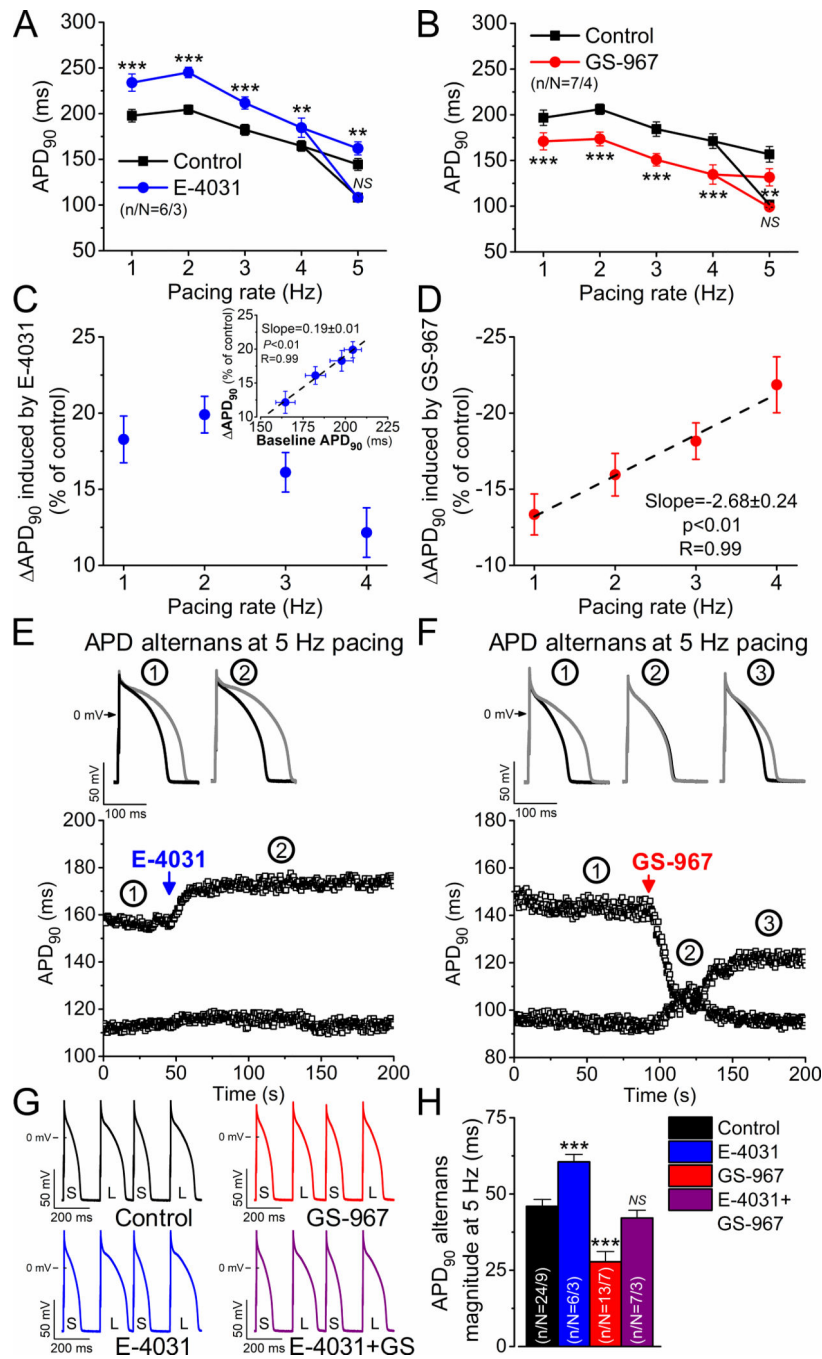
**Figure 4.**

$I_{K_r}$  and  $I_{NaL}$  counterbalance each other on shaping the ventricular action potential (AP). **A**,  $I_{NaL}$  inhibition (GS-967, 1  $\mu$ mol/L) abolished AP duration (APD) prolongation induced by  $I_{K_r}$  blockade (E-4031, 1  $\mu$ mol/L). **B**,  $I_{K_r}$  inhibition reverts APD shortening induced by  $I_{NaL}$  blockade. **C**,  $I_{NaL}$  inhibition abolished AP prolongation caused by modulated  $Na^+$  channel inactivation using anemone toxin II (ATX-II, 5 nmol/L). **D**,  $I_{NaL}$  inhibition abolished AP prolongation in heart failure (HF). APDs at different phases of repolarization are shown below the representative AP traces. Cells were paced at 2 Hz. **E-H**, Plateau<sub>75</sub> potential and maximal rate of repolarization ( $-dV/dt_{max}$ ). Mean $\pm$ SEM is shown.  $n/N$  refers to cells/animals measured in each group. ANOVA with Bonferroni posttest. NS, not significant ( $P>0.05$ ), \* $P<0.05$ , \*\* $P<0.01$ , \*\*\* $P<0.001$  versus control; † $P<0.05$  versus HF.



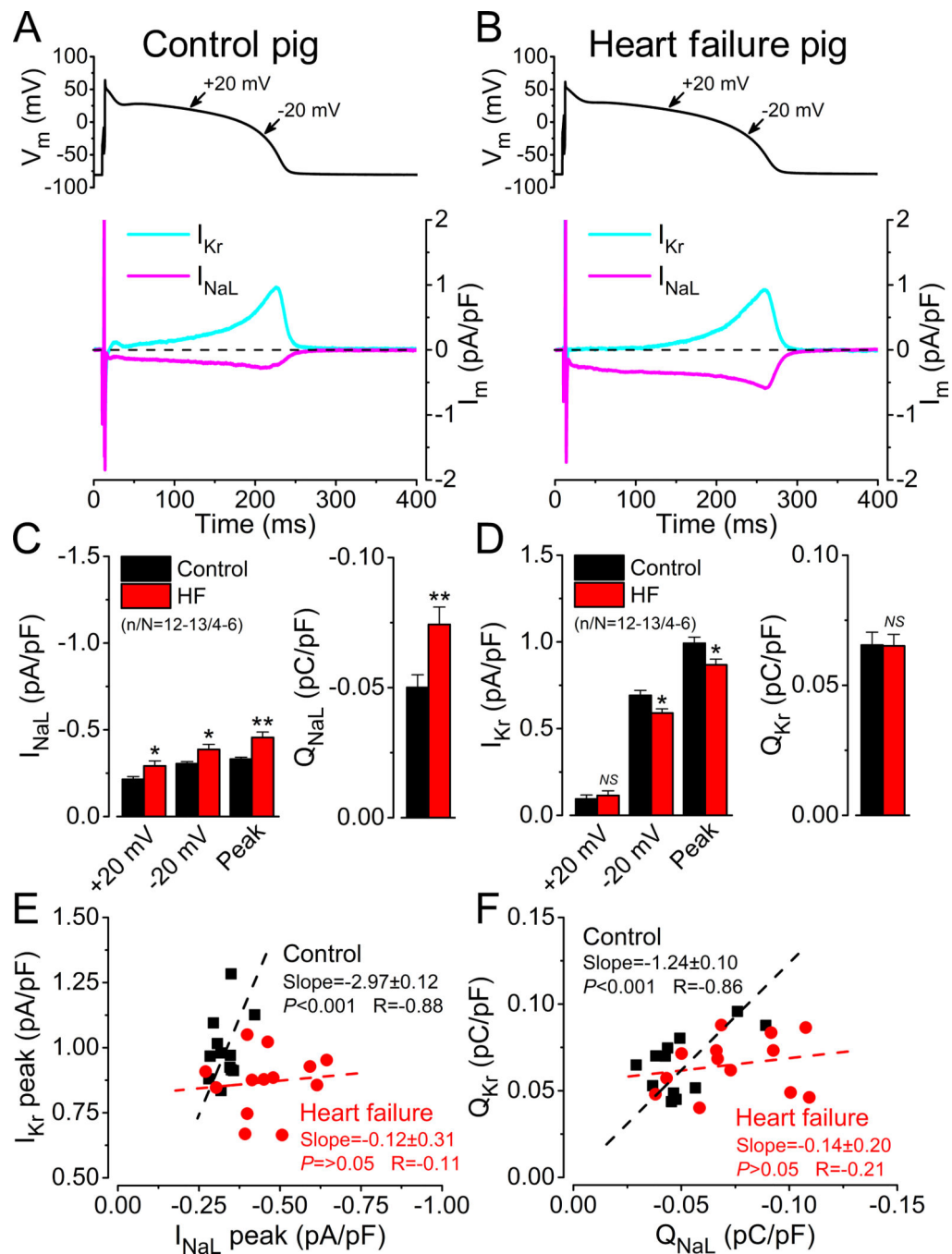
**Figure 5.**

Impact of  $I_{K_r}$  and  $I_{NaL}$  on beat-to-beat and short-term variabilities of action potential duration (APD). **A-D**, Representative AP series and Poincaré plots constructed using 50 consecutive APs at steady-state 2 Hz pacing. Inset shows the short-term variability (STV) of APD. **E-H**, Cumulative distribution curves of beat-to-beat changes in APD.  $I_{K_r}$  inhibition (E-4031, 1  $\mu\text{mol/L}$ ),  $I_{NaL}$  enhancement (ATX-II, 5 nmol/L) and heart failure (HF) increased APD-variability, whereas  $I_{NaL}$  inhibition (GS-967, 1  $\mu\text{mol/L}$ ) significantly reduced APD-variability. Insets show the number of APs having more than 5 and 10 ms beat-to-beat variability of APD. Mean $\pm$ SEM is shown.  $n/N$  refers to cells/animals measured in each group. ANOVA with Bonferroni posttest. NS, not significant ( $P>0.05$ ), \* $P<0.05$ , \*\* $P<0.01$ , \*\*\* $P<0.001$  versus control; †† $P<0.01$ , ††† $P<0.001$  versus HF.



**Figure 6.** Frequency-dependent effect of  $I_{K_r}$  and  $I_{NaL}$  inhibition on action potential duration (APD). **A**, Frequency-dependence of  $I_{K_r}$  inhibition. **B**, Frequency-dependence of  $I_{NaL}$  inhibition. **C**, Frequency-dependence of the E-4031-induced change in APD. Inset shows the correlation between the E-4031-induced change in APD and the baseline APD. **D**, Correlation between the pacing rate and GS-967-induced change in APD. Dashed line represents the fitted linear regression curve. **E** and **F**, Timing of E-4031 (1  $\mu$ mol/L) and GS-967 (1  $\mu$ mol/L) effects on APD alternans at 5 Hz steady-state pacing. Insets show representative APs at time points

indicated. **G** and **H**, Representative AP series and APD alternans magnitudes. (S and L refer to short and long APDs, respectively.) Mean $\pm$ SEM is shown.  $n/N$  refers to cells/animals measured in each group. Paired Student  $t$  test. *NS*, not significant ( $P>0.05$ ), \*\* $P<0.01$ , \*\*\* $P<0.001$ .

**Figure 7.**

$I_{Kr}$  and  $I_{NaL}$  in control and ischemic HF porcine ventricular myocytes under self action potential (AP)-clamp. **A** and **B**,  $I_{Kr}$  and  $I_{NaL}$  in porcine ventricular cardiomyocytes under self AP-clamp in control and ischemic heart failure (HF) induced by chronic myocardial infarction (5-month post-MI).  $I_{NaL}$  and  $I_{Kr}$  were measured as 1  $\mu\text{mol/L}$  GS-967 and 1  $\mu\text{mol/L}$  E-4031-sensitive currents under self AP-clamp, respectively. Cells were paced at 1 Hz. **C** and **D**,  $I_{NaL}$  and  $I_{Kr}$  densities and net charges in control and HF. **E** and **F**, Correlation between  $I_{Kr}$  and  $I_{NaL}$  peak densities and net charges under self AP-clamp. Dashed lines

represent the fitted linear regression curves. Mean $\pm$ SEM is shown.  $n/N$  refers to cells/ animals measured in each group. ANOVA with Bonferroni posttest. *NS*, not significant ( $P>0.05$ ), \* $P<0.05$ , \*\* $P<0.01$ .